Stochastic in Space and Time: Part 1, Characterizing Orographic Gradients in Mean Runoff and Daily Runoff Variability

A.M. Forte[1] and M.W. Rossi[2]

[1] Department of Geology and Geophysics, Louisiana State University, Baton Rouge, Louisiana, USA.

[2] Earth Lab, Cooperative Institute for Research in Environmental Sciences (CIRES), University of Colorado, Boulder, Colorado, USA.

Corresponding author: Adam M. Forte (aforte8@lsu.edu)

Key Points:

- WaterGAP3 water model data overestimates daily runoff variability in snowmelt influenced watersheds
- Global relationships between mean runoff and daily runoff variability are strongly mediated by snowmelt fraction
- Topographic drivers of mean runoff, snowmelt fraction, and daily runoff variability are best assessed at the mountain range scale

Abstract

Mountain topography alters the phase, amount, and spatial distribution of precipitation. Past efforts focused on how orographic precipitation can alter spatial patterns in mean runoff , with less emphasis on how time-varying runoff statistics may also vary with topography. Given the importance of the magnitude and frequency of runoff events to fluvial erosion, we evaluate whether orographic patterns in mean runoff and daily runoff variability can be constrained using the global WaterGAP3 water model data. Model runoff data is validated against observational data in the contiguous United States, showing agreement with mean runoff in all settings and daily runoff variability in settings where rainfall-runoff predominates. In snowmelt-influenced settings, runoff variability is overestimated by the water model data. Cognizant of these limitations, we use the water model data to develop relationships between mean runoff and daily runoff variability and how these are mediated by snowmelt fraction in mountain topography globally. A global analysis of topographic controls on hydro-climatic variables using a Random Forest Model were ambiguous. Instead, relationships between topography and runoff parameters are better assessed at mountain range scale. Rulesets linking topography to mean runoff and snowmelt fraction are developed for three mid-latitude mountain landscapes—British Columbia, European Alps, and Greater Caucasus. Increasing topographic elevation and relief together leads to higher mean runoff and lower runoff variability due to the increasing contribution of snowmelt. The three sets of empirical relationships developed here serve as the basis for a suite of numerical experiments in our companion manuscript (Part 2).

Plain Language Summary

It has long been understood that mountain ranges can have profound influences on the location and intensity of precipitation, for example through the formation of rain shadows. Less clear is how these "orographic effects" are reflected in the details of river runoff, specifically how much runoff varies from day-to-day. Understanding this variability of runoff is important as differences in variability directly influence how rivers respond to changes in rock uplift rate. Here we use results from a global water model integrated with topography data to explore how runoff variability is related to topography in high relief landscapes. Consistent with prior work, we find and expand on the observation that mean runoff and runoff variability are inversely correlated and that the nature of their relation fundamentally depends on how much runoff comes from snowmelt as opposed to rain. In turn, both mean runoff and the importance of snowmelt are positively correlated with aspects of topography. Our results imply that incorporating variability into models of coupled developing orographic patterns in runoff and landscape evolution is critical and we identify a simple framework within which to develop such models. Examples of these models are presented in a companion work (Part 2).

1 Introduction

Weather systems develop over the course of hours to weeks depending on their size (e.g., Trenberth et al., 2003), while landscapes evolve over millennia and longer. Climatic drivers of the long-term evolution of mountain belts (Whipple, 2009) are impeded by this mismatch in timescale. Modeling weather and hydrology over long timescales is a substantial computational challenge (e.g., Shen et al., 2021), and thus the choices made in representation of the hydro-climate are often baked into the simplified process laws we use to construct landscape evolution models. For fluvial landscapes, the most widely used model for river incision and relief

development is the stream power model (Howard, 1994; Whipple & Tucker, 1999). The details of this model have been expounded elsewhere (e.g., see reviews in Kirby & Whipple, 2012; Lague, 2014; Whipple et al., 2022; Whipple & Tucker, 1999; Whittaker, 2012) and we present a more complete synopsis in Part 2. In short the shear stress formulation of stream power asserts that fluvial erosion can be expressed as the product of three terms: a coefficient describing the efficiency of erosion, drainage area raised to an exponent, and local slope raised to another exponent. The latter two terms and the ratio of the exponents can be constrained using topographic data alone (e.g., Wobus et al., 2006), leaving the coefficient of erosion and the value of the slope exponent to account for a large number of important process parameters including climate. While unpacking the assumptions underlying generalized forms of stream power have been addressed by many papers (e.g., Kirby & Whipple, 2012; Lague, 2014; Whipple et al., 2022), we highlight two sets of assumptions of stream power that motivate our analysis of global runoff data. First, it is common to use drainage area as a proxy for discharge. Orographic precipitation (Galewsky, 2009; Roe, 2005) is mimicked in 1D stream power models by adding an additional area dependence on runoff that alters concavity (Roe et al., 2002) and fluvial relief (Roe et al., 2003). In 2D, these basic effects tend to be more ambiguous (Han et al., 2014) and produce discordance between mainstem and tributary morphology (Leonard & Whipple, 2021). Second, simple stream power typically assumes a characteristic discharge, thus entailing either that erosion thresholds are negligible or that the effects of thresholds are subsumed within the stream power parameters itself. This latter possibility has now been carefully examined by changing the temporal scale over which river erosion is modeled (i.e., at the daily scale). By integrating stream power over the probability distribution of flows above erosional thresholds (Lague et al., 2005; Snyder et al., 2003; Tucker, 2004; Tucker & Bras, 2000), the response of

river profiles to climate is not only embedded in the coefficient of erosion but also the effective slope exponent (DiBiase & Whipple, 2011; Lague, 2014). While the roles of both orographic precipitation and stochastic climate on stream power have each generated a lot of study on their own, there has been less effort examining them together.

Integrating orographic effects with stochastic runoff into stream power models requires better constraints on how mean runoff and runoff variability are related (or unrelated) to each other via topography. Prior studies show that mean runoff and the shape of daily runoff distributions are correlated with each other in rainfall-dominated systems (Molnar et al., 2006; Rossi et al., 2016). Figure 1B illustrates this for contiguous United States using streamflow data from select watersheds where the impact of human disturbance and management has been minimized (Figure 1A). To select watersheds to motivate and validate the global water model data that we use for the majority of this effort (described in greater detail later), we used the Geospatial Attributes of Gages for Evaluating Streamflow (GAGES-II) reference gauges and the Hydro-Climatic Data Network (HCDN-2009). HCDN-2009 is a subset of GAGES-II and thus includes a smaller number of sites. Details for selection of those stations used for validation are described below along with how we derived the shape parameters of each distribution. However, note here that higher shape parameters shown in Figure 1 indicate lower runoff variability. The empirical data split into two broad relationships. Separation of the two trends appears to correspond to mean annual temperatures of around 0-10° C (Figure 1B), which we hypothesize is due to relatively small changes in the fraction of mean annual streamflow that is derived from snowmelt. While prior work has examined how orographic patterns in the spatial distribution of snow alters stream power predictions (Anders et al., 2008), we are not aware of any studies showing how snowmelt alters stochastic runoff and stream power predictions. As such, coupled

models of climate and tectonics using stream power (e.g., Beaumont et al., 1992; Willett, 1999) may be missing important feedbacks between topographic relief and snowmelt as mountain ranges grow.

The lack of focus on integrating orographic precipitation and stochastic runoff into stream power models is likely due to data limitations and the dearth of simple hydrological relations that can be upscaled to landscape evolution timescales. Precipitation observations provide a starting point, though simplifying water inputs into streamflow outputs are riddled with nonlinearities that can be hard to generalize. Rainfall runoff is nonlinear due to scaling properties within watersheds and dynamical nonlinearities in hillslope runoff generation (e.g., Sivapalan et al., 2002). Furthermore, the relative contribution of different runoff generation mechanisms (i.e., extreme precipitation, soil moisture excess, snowmelt) to flood frequency is only beginning to be characterized under modern climate conditions (e.g., Berghuijs et al., 2019), let alone for time-varying ones. Process-based hydrological models help unpack these nonlinearities for a given setting (Fatichi et al., 2016), but are typically applied at small spatial scales. Our approach is to use a global water model (Alcamo et al., 2003; Döll et al., 2003) to help constrain how topography, runoff generation, and streamflow statistics can be generalized for river incision modeling more broadly.

2 Background

2.1 Orographic effects

Topography perturbs the equilibrium structure of the atmosphere by adding roughness, obstructing air masses, and serving as a heat source (Smith, 1979). The conventional treatment of orographic precipitation in landscape evolution studies (e.g., Beaumont et al., 1992; Willett,

1999) focuses on the thermodynamic implications of mountain topography on how precipitation is extracted from the atmosphere via forced ascent. The saturation vapor pressure of water in air is related to its temperature via the Clausius-Clapeyron equation (see review in Roe, 2005). As air masses move up and over mountain topography, precipitation on windward slopes increases as partially saturated air cools during ascent. A 'rain shadow' subsequently develops when the relatively drier air descends and warms on leeward slopes. This first-order description is well-rooted in atmospheric physics and observations (Barros & Lettenmaier, 1994). To extend these dynamics to air parcels flowing over more complex terrain, Smith & Barstad (2004) developed a linear model of orographic precipitation that accounts for atmospheric dynamics, upwind advection, and downslope evaporation. In this context, linearity does not refer to a single function describing rainfall but is instead a property of the system of differential equations used such that they are analytically tractable. Because settling velocities of snow are an order of magnitude lower than rain, this model can be used to examine how snow alters the spatial distribution of water inputs (Anders et al., 2008). However, one notable limitation to the linear model of orographic precipitation is that it does not account for the blocking of air by terrain, a nonlinear process that depends on the Brunt-Vaisala frequency describing the horizontal propagation of waves, horizontal windspeed, and orogen-scale relief (Barros & Lettenmaier, 1994; Galewsky, 2009; Jiang, 2003). Given that one of the key targets of landscape evolution models is to couple topography to climate through time, linear models of orographic precipitation are perhaps best suited to smaller mountain ranges.

Another approach towards characterizing orographic precipitation is to use climatological observations, especially since the advent of satellite-based remote sensing. For example, the Tropical Rainfall Measuring Mission (TRMM) was spaceborne for 17 years and provided new

insights into complex spatial patterns in rainfall set up by high topography (e.g., Bookhagen & Burbank, 2006; Bookhagen & Strecker, 2008; Deal et al., 2017; Forte et al., 2016; Nesbitt & Anders, 2009). One of the key insights from these studies is the central importance of local relief to driving spatial patterns in rainfall. For example, in the Himalaya, TRMM rainfall revealed two narrow bands of rainfall that correspond to abrupt physiographic transitions into the Lesser Himalaya and into the Greater Himalaya which had not been previously identified (Bookhagen & Burbank, 2006, 2010). As such, spatial patterns derived from TRMM rainfall are increasingly being used to inform interpretations of river channel profiles (Adams et al., 2020; Bookhagen & Strecker, 2011; Leonard et al., 2023), though these approaches typically assume mean rainfall is directly proportional mean runoff. While other remote sensing products like MODIS can also help constrain snow cover to construct a full water budget (Bookhagen & Burbank, 2010), such products tend to require temperature-index or process-based hydrological models to reliably estimate snowmelt contributions to streamflow (Walter et al., 2005).

Given the importance of snowmelt to streamflow in mid-latitude mountain ranges (Barnett et al., 2005; Barnhart et al., 2016), the difficulty of obtaining direct estimates of snowmelt leads to substantial uncertainty when using remotely sensed rainfall data as a proxy for runoff. Altering the phase of precipitation can cause up to 100% reductions in snowmelt contributions to streamflow in settings near the freezing temperature window (Adam et al., 2009). This has prompted some authors to suggest that climate change driven reductions in snowmelt fraction generally leads to lower streamflow as snowfall gives way to rain (Berghuijs et al., 2014). Such arguments rest on the premise that snowmelt runoff will lead to higher runoff ratios, all other things being equal, because solid water is stored in the snowpack and released more slowly than rainfall runoff. Better understanding of orographic effects on the snowmelt

175 contribution to streamflow in mountain landscapes is sorely needed to improve stream power
176 models of river incision.

177 2.2 Stochastic river incision

178 Early efforts to integrate stochastic hydrology into stream power models of river incision
179 (Snyder et al., 2003; Tucker, 2004; Tucker & Bras, 2000) were based on the pioneering work of
180 Eagleson (1978). By simulating rainfall events as Poisson distributions of intensities, durations,
181 and inter-storm periods, rainfall events were represented as rectangular pulses that can be
182 converted to runoff and routed across the landscape in order to evaluate the impact erosion
183 thresholds on landscape evolution. Complementary efforts by Lague et al. (2005) chose to
184 simulate streamflow directly at the daily time step using the stochastic 'precipiton' model. This
185 model considers the time travel distribution of quanta of precipitation that produces runoff and
186 generates daily streamflow distributions that follow an inverse gamma distribution (Crave &
187 Davy, 2001).

188 Despite the differences in the hydrologic assumptions made by these early modeling
189 efforts, together they highlighted the need for adding stochastic events to stream power in order
190 to interpret the long-term evolution of river profiles. Under this view, the steady state form of
191 river profiles was no longer a simple function of mean climate, but instead reflected the complex
192 interplay between the frequency of large flows and erosional thresholds set by coarse sediment
193 (Shobe et al., 2016) and the detachment of bedrock (Whipple et al., 2000). While the overall
194 approach of these efforts was similar, the functional form of probability distributions of
195 streamflow differed. The use of daily data, while insufficient for short-duration flash floods,
196 balances important tradeoffs in characterizing magnitude-frequency relationships while also
197 being tractable to simulate over landscape evolution timescales. Poisson rectangular pulses

always generate light-tailed, exponential, daily runoff distributions while the inverse gamma distribution is able to produce heavy-tailed distributions that do not have a finite variance, depending on the value of shape parameter. There is still an open question as to how heavy-tailed streamflow distributions truly are (Malamud & Turcotte, 2006; Molnar et al., 2006), though the advantage of adopting these stochastic frameworks is that they are well-suited to simulating both frequent and infrequent flows and thus determining the geomorphically effective event (Huang & Niemann, 2006). Rossi et al. (2016) recently suggested that the stretched exponential, or Weibull, distribution provides a flexible probability distribution that spans light-tailed to apparently heavy-tailed distributions (Laherrère & Sornette, 1998), and thus is what we choose to fit observed and model runoff daily runoff data below.

Regardless of how stochastic processes are represented, these early efforts prompted a large number of studies to take a closer look at whether relationships between long-term erosion rates and river morphology can be better explained using stochastic-threshold models of river incision (Campforts et al., 2020; Desormeaux et al., 2022; DiBiase & Whipple, 2011; Forte et al., 2022; Scherler et al., 2017). While success is decidedly mixed, the general outcome of using stochastic-threshold models has been to provide an alternative interpretation to nonlinear relationships between river channel morphology and long-term erosion rates (Harel et al., 2016; Marder & Gallen, 2023). In these cases, nonlinear relationships between river morphology and long-term erosion rates arise because erosional thresholds are exceeded more frequently as erosion rate and relief increase. The climate driver on river profile evolution is not mean annual precipitation itself, but how the soil water balance (Deal et al., 2018) and the hydrologic structure of watersheds (Basso et al., 2023) mediate flood frequency. These concepts place the central focus on water storage-discharge relationships (Botter et al., 2009; Kirchner, 2009) to condition

how rainfall events are converted to runoff ones. The same kind of framework can be used to account for seasonal snowmelt contributions to streamflow (Schaefli et al., 2013).

3 Datasets

Our overarching goal is to better parameterize 1D models of fluvial profile evolution that account for both stochastic events and orographic controls on runoff generation. Model development is the focus of our companion manuscript (Forte & Rossi, 2023). The focus of this manuscript is on developing empirical relationships between topography and daily runoff statistics in mountain settings. Note that runoff and streamflow, i.e., discharge, are not synonymous terms. For empirical data, streamflow data are typically what is measured and runoff is inferred by normalizing the data by drainage area. For water model data, runoffs are simulated directly. We primarily rely on three datasets: (1) a daily, global water model derived from climate reanalysis data (WaterGAP3 data including daily runoff), (2) observational stream gauge data from the contiguous United States (HCDN-2009 daily streamflow), and (3) near global topographic data (SRTM-90 and derived HydroSHEDS v1 gridded elevation).

3.1 Hydrology Data

Because streamflow data availability and quality is globally variable, we sought a single global runoff dataset that could be used to interrogate modern relationships among topography, snowmelt, and runoff. We used the Water Global Assessment and Prognosis (WaterGAP3), the most recent version of a 20+ year old global water model (Alcamo et al., 2003; Döll et al., 2003). WaterGAP3 improves on prior versions by increasing the spatial resolution from the original 0.5° to 0.25° pixel size (Eisner, 2015) and is one model included in the Earth2Observe Water

Resource Reanalysis project (Schellekens et al., 2017). These model data have broad utility (e.g., Schmied et al., 2014), including for parameterization of stochastic-threshold incision models (STIM) of river incision (Campforts et al., 2020). For this analysis, we downloaded the global, 20-year, daily time series from the Earth2Observe portal (www.earth2observe.eu; last accessed April 8, 2022) spanning from January 1, 1980 to December 31, 1999. Daily data represent the mean value of each variable for each day.

For each pixel and day, WaterGAP3 contains a large number of input and derived hydro-climatological parameters including precipitation, runoff, discharge, and evapotranspiration. We primarily focus on the derived runoff variables from WaterGAP3, but also briefly consider temperature and precipitation. Daily average surface temperature is not distributed with WaterGAP3, so we rely on another reanalysis product of identical resolution from the Earth2Observe set, namely SURFEX-TRIP (Decharme et al., 2010, 2013). Surface temperature data are used to help interpret variation we see within the WaterGAP3 runoff data. Runoff data are subdivided into three components in WaterGAP3: surface runoff (R_s), subsurface runoff (R_{sb}), and snowmelt (R_{sm}), where total daily runoff (R_t) is the sum of the three. In the original WaterGAP3 dataset, all of these components of runoff are denoted with the variable 'Q'. We do not use this notation here given the common association of Q with discharge [L^3/t] as opposed to runoff [L/t]. For each pixel across the time-series, we calculated mean daily runoff ($\bar{R}_t$), mean daily precipitation ($\bar{P}$), means of each of the three runoff components ($\bar{R}_s$, $\bar{R}_{sb}$, $\bar{R}_{sm}$), and Weibull shape (c) and scale (R_0) parameters of the daily total runoff distributions (see section 4.1 for details). Given our interest in probing the importance of snowmelt, we also calculated the fraction of runoff contributed by snowmelt (SF), where:

$$SF = \frac{\overline{R_{sm}}}{\bar{R}_t} \quad (1)$$

Similarly, we calculate baseflow fraction of runoff (BF), where:

$$BF = \frac{\overline{R_{sb}}}{\overline{R_t}} \quad (2)$$

that we use to exclude watersheds with a substantial groundwater component to its daily fluxes.

To validate model runoff data, we used observational streamflow data from the Hydro-Climatic Data Network – 2009 (HCDN-2009) (Lins, 2012). These 743 stream gauges were identified by the USGS to be high quality, long, continuous records for watersheds with minimal impact by humans (e.g., due to landcover change, dams, and diversions). We downloaded streamflow data from the National Water Information System (NWIS) server for the dates between January 1, 1980 and December 31, 1999, to directly compare to the WaterGAP3 data. During the processing of individual HCDN-2009 time series data, any day that included provisional data or data where there was an extra qualifier on the quality (e.g., 'ICE') was removed and treated as NaN data. We characterize the completeness of the time series by dividing the number of days with reliable data by the total number of days. Because HCDN-2009 stream gauges are a subset of the reference stations in the Gages for Evaluating Streamflow version II (GAGES-II) network, we were able to use watershed boundaries provided by Falcone et al. (2011) to calculate watershed-averaged properties and normalize streamflow by drainage area. This latter calculation was used as an estimate for daily runoff. Processing and validation of the WaterGAP3 runoff model against HCDN-2009 observations is described in section 4.2.

3.2. Topography Data

Because we are focused on how hydroclimatic parameters vary with topography in mountain settings, it is necessary to pair the WaterGAP3 data with a global topographic dataset. We largely used the HydroSheds v1, 15-arcsecond, digital elevation model that is derived from SRTM elevation data (Lehner et al., 2008). We also used the higher resolution SRTM-90 data (Farr et al., 2007) for watershed delineation when validating WaterGAP3 against HCDN-2009 data. The HydroSheds v1 topographic data are used for two purposes: (1) To screen for portions of the global surface where orographic feedbacks with climate are relevant, and (2) To develop empirical relationships between topography and runoff statistics. With respect to data screening, we only used WaterGAP3 data where the mean elevations are greater than 250 meters above sea level and where local reliefs are greater than 500 meters. To calculate local relief at a fixed scale, we first reprojected the global geographic DEM into an equal area cylindrical projection and then calculated local relief within a 2.5 km radius circular moving window. This is a scale that prior studies have shown to linearly correlate with river channel steepness (e.g., DiBiase et al., 2010), and thus expect it to be well suited to developing empirical relationships between river morphology and local relief. After the relief calculation, we projected the data back into the original WGS 84 geographic coordinate system to facilitate calculation and comparisons with the rest of the datasets that were also in geographic coordinate systems. The initial screening of the WaterGAP3 data using local relief is then further filtered to exclude pixels where baseflow (eq. 2) exceeds 0.25, with an eye towards minimizing the confounding factor of large groundwater contributions. To develop relationships between topography and runoff statistics we record minimum, mean, and maximum elevations within a WaterGAP3 pixel and the mean local relief

within a WaterGAP3 pixel as calculated from the enclosed 60 HydroSheds pixels (i.e., there are 60 HydroShed pixels within each WaterGAP3 pixel).

4 Data Analysis

To develop empirical relationships between topography and runoff statistics from WaterGAP3, it was first important to figure out at which scale such relationships might emerge. To this end, we conduct both a global analysis and a set of regional ones that broadly correspond to the mountain range scale. These empirical relationships serve as the basis for the model development and analysis we conduct in Part 2 (Forte & Rossi, 2023). There are four main steps to the data analysis: (1) Characterization of statistical parameters for daily runoff; (2) Validation of WaterGAP3 model derived parameters with HCDN-2009 stream gage observations; (3) Global assessment of topographic controls on runoff, runoff variability, and snowmelt fraction, and (4) Development of regionally-based relationships between topographic metrics and runoff statistics.

4.1. Daily Distributions

A number of probability distributions have been considered for the problem of bedrock river incision, including exponential (Snyder et al., 2003; Tucker, 2004), power law (Molnar et al., 2006), inverse gamma (Campforts et al., 2020; DiBiase & Whipple, 2011; Lague et al., 2005; Scherler et al., 2017) and Weibull (Forte et al., 2022; Rossi et al., 2016) distributions. We follow Rossi et al., (2016) and use a two-parameter Weibull distribution to fit the right tail of the daily runoff distribution above a threshold value. Choosing thresholds to fit empirical distributions is a notoriously vexing challenge (e.g., Dupuis, 1998) and makes it more challenging to implement in numerical models (see Forte & Rossi, 2023), though it enables better fidelity to the observed

right tail. For this analysis, the threshold is treated as a third parameter that is held constant across sites to enable comparison of fit parameters. Above the threshold, distributions are described by a shape parameter (c_x) that describes daily variability and a scale (x_0) parameter related to the mean of the distribution, where:

$$pdf(x; x_0, c_x) = \frac{c_x}{x_0}\left(\frac{x}{x_0}\right)^{c_x-1} exp^{-1(x/x_0)^{c_x}} \quad (3)$$

Because we are only fitting the right tail of the distribution, the parametric mean and the empirical mean need not match. The mismatch between the two is a measure of how well tail fitting is able to represent the full distribution. We use the fit parameters to characterize both daily precipitation (p_0, c_p) and daily runoff (r_0, c_r). Interpretations of fit parameters primarily focus on the shape parameter because it describes the right tail of daily values, which we colloquially refer to as the variability. Larger values of c_x indicate lower variability (i.e., smaller relative differences between daily runoff values), where c_x=1 is equivalent to the exponential distribution. The need for three parameters and the inability to analytically integrate the product of this distribution with stream power is not ideal, posing important challenges to numerical simulations of bedrock rivers (Forte & Rossi, 2023).

To estimate shape parameters, we follow Wilson & Toumi (2005) and perform a linear fit on the natural log linearized right tail of the exceedance frequency distribution above a threshold. On the transformed data, the shape parameter, c_x, is the slope of the regression, and the scale parameter, x_0, is exp(-intercept/slope) of the regression. Because parametric fits will be sensitive to threshold choice, distribution parameters were calculated using two thresholds for the daily runoff data, the upper 5% and upper 1% of daily values. These thresholds reflect a compromise between fitting the majority of flows while also honoring the right tail, the latter of which

dictates the nonlinear relationship between channel steepness and long-term erosion rates. Figures and discussion are based on the 1% threshold for both runoff and precipitation distributions. This corresponds to the event magnitude that happens 3-4 times per year. While threshold choice did alter the best-fit values for c_r, suggesting that a simple Weibull distribution is not able to fully characterize all cases, this variation in c_r did not substantially alter the relative spatial patterns in the shape of the right tail. Runoff parameters were calculated on both the daily streamflow data (HCDN-2009) and the daily total runoff data from WaterGAP3. Pixel-based values in WaterGAP3 are not directly comparable to the watershed-averaged ones in HCDN-2009. In the following section, we address this challenge in the context of validating water model runoff data against observations.

4.2. Runoff Parameter Validation

Prior validation of WaterGAP3 data suggests that model data robustly reproduce mean river discharge from gauging stations (Beck et al., 2017; Eisner, 2015; Schmied et al., 2014, 2020). None of these prior assessments considered how well daily runoff variability is represented. Given the importance of daily runoff variability to bedrock river incision modeling, it is thus important to assess the extent to which shape parameters calculated from WaterGAP3 are consistent with those observed at stream gauges. For the sake of comparison, we first screened the HCDN-2009 network using the same topographic criteria used to screen WaterGAP3. Namely, we excluded watersheds where catchment relief (i.e., maximum minus minimum elevation within the catchment) is less than 500 meters and where mean elevation is less than 250 meters. Of the retained sites, we also imposed the additional criterion that HCDN-2009 daily runoff records are >95% complete within the WaterGAP3 time period (January 1,

1980 - December 31, 1999). We also removed data that occurs on leap days because these days are not calculated in the WaterGAP3 time series.

Once candidate HCDN-2009 stations were identified for validation, we needed to process the WaterGAP3 data to enable fair comparison. The first approach uses the mean runoff and runoff variability parameters calculated for each pixel in WaterGAP3. By oversampling these raster datasets of stochastic parameters to 1.5 seconds per pixel, HCDN-2009 watershed boundaries were used to calculate spatially averaged values of runoff parameters. While this treatment may be valid for small HCDN-2009 watersheds of similar scale to the WaterGAP3 pixels, this calculation may be problematic for larger watersheds where runoff should be routed downstream. As such, the second approach uses watershed boundaries to clip and route the WaterGAP3 data for each day within the 20-year time series. The mean runoff and shape parameter of the routed data are then calculated for the daily, routed data at the river outlet. For this computationally intensive approach, we used TopoToolbox (Schwanghart & Scherler, 2014) to: (1) acquire SRTM-90 digital elevation models (DEMs) for each watershed via the OpenTopography API, (2) project each DEM to the Universal Transverse Mercator (UTM) projection, (3) clip each day of the WaterGAP3 data to the watershed boundary and resample to the resolution of the DEM, (4) route discharge through the basin to build a time series of daily runoff at the outlet of each watershed, and (5) calculate mean runoff and shape parameters for the outlet time series.

4.3. Global Analysis

After understanding the strengths and limitations of WaterGAP3, these model data were used to identify the strongest predictors of mean runoff and daily runoff variability globally. The global analysis used two complementary approaches: (1) Develop relationships between mean

runoff and variability (e.g., Molnar et al., 2006; Rossi et al., 2016), in a way that can account for the potential influence of snowmelt, and (2) Use unsupervised machine learning to probe the WaterGAP3 data and help identify strong predictors of mean runoff, snowmelt, and runoff variability.

For the first approach, we used the snowmelt fraction (Eq. 1) to partition the filtered WaterGAP3 data (see Section 3.1) into bins. Within each bin, we fit both a linear and a power law function relating mean runoff and the shape parameters of each pixel within that bin. This approach was motivated by empirical (Rossi et al., 2016) and ecohydrological modeling (Deal et al., 2018) studies that show how climatically driven gradients in daily runoff variability differ between rainfall-runoff and snowmelt-runoff regimes. For example, Rossi et al. (2016) showed that watersheds with lower snowmelt contributions were better described by a power law relationship between mean runoff and its associated Weibull shape parameter. In contrast, regions with higher snowmelt contributions showed a more linear relationship between these parameters. To compare the fits of both functions, we consider both the RMSE and the reduced chi-squared statistic under the view that that minimization of RMSE and/or reducing the chi-squared statistic closer to one should indicate the 'better' fit to the data.

In the second approach, we consider a larger suite of hydro-climatological, topographic, and geographic variables. Random forest regression (RFR) was used to assess the relative importance of potential predictor variables with respect to a given 'target' variable (Grömping, 2009). Target variables are hydro-climatic ones chosen based on their potential relevance to relationship between mean runoff and runoff variability (i.e., mean temperature, mean precipitation, mean runoff, daily runoff variability, and snowmelt fraction). The list of predictor variables are broader and varied according to each target. Predictor variables included

topographic (mean elevation, maximum elevation, mean local relief), geographic (latitude), and hydro-climatic (mean temperature, mean precipitation, daily precipitation variability, mean runoff, daily runoff variability, and snowmelt fraction) variables. We also attempted to thin predictor variables and remove what amounts to duplicates, e.g., as described in the results, latitude is the primary predictor of mean annual temperature and thus for other RFRs, we only include MAT as opposed to both MAT and latitude. Ultimately, we are not interested in the prediction per se, but to use the RFR to help identify which variables emerge as the most viable candidates linking mean runoff, snowmelt fraction, and daily runoff variability. In particular, we sought to discover which and whether any of the topographic metrics can be used to generalize hydro-climatic relationships that may co-evolve with growing topography. To perform the RFR, we used the *RandomForestRegressor* within *SciKit-Learn*, using the default values and a seed for the random state of 0.

4.4. Regional Cases

As we discuss in the context of our findings below, the global analysis revealed that generalizable relationships between topography and hydro-climatology were difficult to isolate at this largest spatial scale. While the global analysis reinforced the notion that snowmelt fraction mediates the relationship between mean runoff and daily runoff variability, scatter in these relationships clearly reflect the geographic diversity of montane hydrology. Furthermore, the lack of unambiguous topographic predictors that could be used to build rules for co-evolving stochastic parameters with the growth of mountain ranges limits the utility of the results from the global analysis to the application of 1D bedrock river incision modeling (Forte & Rossi, 2023). As such, we identified relationships between topography and stochastic runoff specific to individual mountain ranges, where differences in regional climate and geography can be partially

accounted for. To begin this regional analysis, we started at first at the global scale and used a 2° rectangular moving window to calculate the Spearman's rank correlation coefficient between candidate topographic variables and hydro-climatological ones. The topographic variables considered were the same as in the global analysis (mean elevation, maximum elevation, and mean local relief). The hydroclimatic variables we focused on were mean runoff and snowmelt fraction, the latter of which can be linked to daily runoff variability using relationships from the global analysis. We opt to focus on snowmelt fraction instead of daily runoff variability directly because one of the hypotheses we are trying to test in the 1D river incision modeling (Forte & Rossi, 2023) is how and whether snowmelt dynamics alter interpretations of stream power based analyses of river profiles. The results of the rank correlation analysis were used as the basis of selecting three regions where well-defined relationships can be developed between topography and hydro-climate. Specifically, these regional cases focus on the mid-latitude mountains of British Columbia, European Alps, and the Greater Caucasus (Figure 2), where snowmelt contributes a sizable fraction of daily streamflow.

5 Results

5.1 Validation of WaterGAP3

Figure 3 summarizes the results from our validation of WaterGAP3 model data against historical observations from select HCDN-2009 stream gages. The mean values for both datasets plot around the 1:1 line without obvious bias (Figure 3A), lending support to prior assessments (e.g., Beck et al., 2017; Eisner, 2015; Schmied et al., 2014, 2020). However, scatter around this relationship shows that a >25% mismatch in mean values is not unusual. In general, simple spatial averaging (closed symbols) performs almost as well as the computationally intensive

routed approach (open symbols), though routing matters for individual cases. From this, we conclude that the HCDN-2009 watersheds are at the appropriate scale for WaterGAP3 validation and that downstream scaling of streamflow statistics is not strongly influencing our parameter estimates. This perhaps not surprising given that the filtered set of HCDN-2009 watersheds used are relatively small (interquartile range of 105-542 km^2), well within the average pixel size of the WaterGAP3 data and typically smaller than the mountain range scale. For lower values of the shape parameter (i.e., higher runoff variability), the correspondence between the observations and the water model is acceptable (Figure 3B). However, for most watersheds, the shape parameters from WaterGAP3 are less than their empirical counterparts (Figure 3B; D) except at higher shape parameters (i.e., lower daily runoff variability). In these cases, WaterGAP3 values are systematically lower than the HCDN-2009 gage data. This implies that WaterGAP3 tends to *overestimate* variability for these watersheds. For the lower variability watersheds, the routed version of WaterGAP3 does slightly improve water model performance (Figure 3B), but does not remove the systematic bias. The residuals of the mismatch between the HCDN-2009 and WaterGAP3 values do not reveal a relationship between the mean and variability (Figure 3C), which might occur if the WaterGAP3 model was systematically altering storage-release relationships in hydrographs (e.g., due to limitations in how hydrologic processes are represented in the model). However, comparison of the residuals of the shape parameter to the mean annual temperature each the watershed (Figure 3D) indicates one possible interpretation for why variability in lower variability watersheds is overestimated in the WaterGAP3 data. The majority of lower variability basins tend to occur in colder settings, suggesting the possibility that snowmelt processes are not being adequately represented in the WaterGAP3 data. This result supports the argument that WaterGAP3 could benefit from improving the partitioning of runoff

into fast and slow components (Eisner, 2015). The direction of the mismatch is consistent with the notion that snow storage and release may not be fully resolved in WaterGAP3 data even though mean runoff is well represented in the water model.

While systematic differences between model and empirical estimates of daily runoff variability is an important limitation to consider, we continue to use WaterGAP3 as our base dataset for a few reasons: (1) It is globally uniform, allowing for comparison of stochastic runoff in diverse settings, and (2) The systematic bias in variability has been quantified so that its effects can be considered. Importantly, the bias in WaterGAP3 estimates of daily runoff variability lead to a *conservative* estimate of the dynamics we are examining in our 1D modeling of bedrock river incision (Forte & Rossi, 2023). Because hypothesized orographic feedbacks induce lower runoff variability as a mountain range grows, thereby increasing the degree of nonlinearity between channel steepness and erosion rate, it is preferable for the underlying rules setting these feedbacks to overestimate variability than the alternative.

5.2 Global relationships (relating mean and variability)

Figures 4-5 summarize the results for how the parametric fit parameters relate to mean runoff after binning the data by snowmelt fraction. Across all bins, WaterGAP3 data show that mean runoffs are inversely related to daily runoff variabilities, consistent with prior studies (e.g., Molnar et al., 2006; Rossi et al., 2016). The large gridded WaterGAP3 dataset allowed us to more systematically explore these relationships at relatively fine (5%) intervals of snowmelt fraction (Figure 4). Each subpanel in Figure 4 is a heatmap showing the density of WaterGAP3 observations of how the best-fit shape parameters relate to the empirical mean. Regressions on the pixel-level data are shown (solid lines show the better fit between linear and power law regressions). HCDN-2009 observational data are also shown as points for reference. Figure 4

511 demonstrates that it would be difficult to constrain these relationships using observational data
512 alone because representation of different snowmelt fractions can be sparse, especially at higher
513 snowmelt fractions. More importantly, it shows that the functional form of the relationship
514 between the mean and variability changes from sublinear to linear with increasing snowmelt
515 fraction. Using Figure 4 as our guide, we identified a snowmelt fraction of 0.35 as the transition
516 where sublinear relationships give way to linear relationships. Note that this transition is higher
517 than the 10% snowmelt threshold used to delineate snowmelt from rainfall-runoff dominated
518 watersheds in Rossi et al. (2016). This disparity likely arises from two factors. First, that prior
519 analysis focused on the snow fraction of precipitation and not the snowmelt fraction of runoff.
520 Second, the sparsity of observations at higher snowmelt fractions in the HCDN-2009 data are not
521 sufficient to define such a threshold.

522 To more succinctly summarize these findings, Figure 5A-B shows the same plots by
523 binning the data above and below a threshold snowmelt fraction of 0.35. The best of the
524 regression lines from Figure 4 are also plotted for reference. Figure 5A-B highlights that
525 individual regressions largely cluster around each other, especially in the domain where they are
526 well constrained by data. It also shows that the relative spread of parameter values is smaller
527 when there is a high fraction of snowmelt. The linear relationships shown at higher snowmelt
528 fractions (Figure 5B) are strongly underestimating the value of the shape parameter as estimated
529 from gaged basins, consistent with validation results (Figure 3B). However, empirical
530 observations still suggest a linear relationship between the empirical mean runoff and the shape
531 of the daily runoff distribution at higher snowmelt fractions.

532 Because empirical means are not equivalent to the mean value implied by parametric fits,
533 Figure S1 reports the mismatch between the scale parameter fit to the data (i.e., above the 1%

534 threshold or ~4 largest floods per year) and the scale parameter implied by the empirical mean.
535 These results are summarized in Figure 5C-D. In general, the parametric fits produce scale
536 parameters that are on par with the empirical means only at low snowmelt fractions. At higher
537 snowmelt fractions, the parametric fits have much higher scale parameters than the empirical
538 mean would imply, thereby suggesting that the Weibull distribution is not doing a good job at
539 describing the full distribution of events. Finding a single distribution to describe empirical data
540 is a well-known problem and poses unique challenges to simulating runoff distributions over
541 landscape evolution timescales, a challenge we tackle in part 2 of this analysis (Forte & Rossi,
542 2023). Nevertheless, by treating all the data in the same way, we show that the functional
543 relationship between daily runoff variability and mean runoff is highly sublinear at low
544 snowmelt fractions, much like shown in previous studies (Molnar et al., 2006; Rossi et al., 2016).
545 At high snowmelt fraction, the relationship becomes more linear, albeit with the caveat that the
546 form of the distribution may also be changing. Our estimates of this transition using WaterGAP3
547 data provide conservative estimates of orographic feedbacks on runoff variability where both the
548 mean and snowmelt fraction are expected to increase as mountain topography grows. It is
549 conservative because biases in the water model data tend to dampen contrasts between rainfall
550 and snowmelt dominated hydrology, and thus our 1D bedrock river incision modeling uses
551 rulesets with weaker feedbacks than might be expected in reality (Forte & Rossi, 2023).

552 While analyzing the global water model data was motivated by prior studies that
553 identified an inverse relationship between mean runoff and daily runoff variability in the
554 contiguous U.S. (Molnar et al., 2006; Rossi et al., 2016), we felt it also important analyze the
555 global data more generically and explore whether hydro-climatic parameters can be linked to
556 topography itself. This latter objective is essential to building rules that relate stochastic runoff

parameters to mountain range growth and decay. To this end, we opted to use Random Forest Regression to partition the relative influence of topographic, geographic, and hydro-climatic predictors on a small subset of target variables.

5.3 Global relationships (Random Forest Regression)

Figure 6 summarizes the results of the random forest regression (RFR) analysis performed on global, filtered WaterGAP3 data. While principally interested in understanding the controls on mean runoff (Figure 6E-F), daily runoff variability (Figure 6G-H), and snowmelt fraction (Figure 6I-J), we also consider influences on other hydro-climatological variables that emerged as important determinants of these target variables, specifically mean annual temperature (Figure 6A-B) and mean precipitation (Figure 6C-D). The results of the RFR are not particularly surprising, but do shed some light on potential causal chains that links mean runoff, snowmelt fraction, and daily runoff variability as a mountain range grows.

Mean annual temperature and mean precipitation are the two strongest predictors of both mean runoff and snowmelt fraction, with temperature exerting a stronger influence on snowmelt fraction and precipitation exerting a stronger influence on runoff. Mean runoff is the strongest predictor of the shape of the daily runoff distribution, perhaps explaining why prior efforts have focused on this relationship (e.g., Molnar et al., 2006; Rossi et al., 2016).

Importantly, topographic metrics were weak predictors of all three principal targets (mean runoff, snowmelt fraction, daily runoff variability). This may be due to the fact that topography is expected to exert its influence via precipitation and temperature. To assess this, we also set mean precipitation and temperature as target variables in the RFR. The relative predictive power of three topographic metrics and mean temperature on mean precipitation is

relatively uniform. In contrast, latitude is the strongest predictor of mean temperature with mean elevation providing modest predictive power. At this scale of analysis, topography does not appear to emerge as a strong predictor in the RFR modeling.

To further probe how topographic relationships might be obscured in this global analysis, we binned the pixel-level data by its mean temperature and precipitation, which emerged above as first-order controls on snowmelt fraction and mean runoff. We first removed outlier values using the method described by Doane (1976) where bin boundaries are defined after clipping variables to values below the 99.9^{th} percentile. Membership in a given bin was determined by the mean temperature and precipitation of the pixel in question. Within each temperature-precipitation bin, we calculated Spearman's rank correlation coefficient between one of three topographic metrics (mean elevation, maximum elevation, and mean local relief) and either mean runoff or snowmelt fraction. A correlation coefficient is only calculated if there are at least 10 pixels within a given temperature-precipitation bin and if the significance of the correlation coefficient exceeds the 95% confidence interval. We used Spearman's rank correlation coefficient because it does not assume linear correlation.

Figure 7 summarizes the results of the correlation analysis of WaterGAP3 data after binning by mean temperature and precipitation. The colors in plots show correlations between topography and mean runoff (top row) and correlations between topography and snowmelt fraction (bottom row). Green values indicate strong positive correlations, magenta values indicate strong negative correlations, black values indicate weak to no correlation, and grey values indicate that there was not enough observations in the dataset to evaluate correlation. The patterns in correlation are somewhat difficult to interpret as clusters of strong positive correlation are often adjacent to clusters of strong anti-correlation. Topographic predictors of

mean runoff show little sensible pattern (Figures 7A-C), with a hint of positive correlation between local relief and mean runoff at low values of mean precipitation (Figures 7C). Topographic predictors of snowmelt fraction are also complex with a band of positive correlation for lower mean temperatures next to a band of anti-correlation at higher temperatures (Figures 7D-F). While we hesitate to interpret these subtle patterns, the snowmelt fraction results do suggest that increasing topographic elevation and relief only leads to more snowmelt where temperatures are conducive to it, though why this relation has a slope is not obvious.

As we discuss in more depth in the discussion below, the results from the global analysis suggest that there is no single set of globally applicable 'rules' that relate topography to mean runoff and snowmelt fraction. We suspect this is a consequence of the scale of the analysis (i.e., orographic effects are inherently regional) and the lack of accounting for the predominant direction of weather systems with respect to topography (i.e., steep topography is not distinguished as windward versus leeward). Based on this, we next explore a set of three regional analyses that show more promise in constraining orographic controls on mean runoff and snowmelt fraction.

5.4 Regional relationships of mean runoff and daily runoff variability

Given the challenge of identifying simple relationships between topography (i.e., mean elevation, maximum elevation, and mean local relief) and either mean runoff or snowmelt fraction (Figures 6-7), we now examine whether regional relationships between these variables are being obscured by the global treatment. Of the six relationships shown in Figure 7, the relationship between local relief and mean runoff and the relationship between maximum elevation and snowmelt fraction seemed the most promising when evaluated spatially. Figure 8 summarizes the sign and strength of these relationships for all WaterGAP3 data that meet our

selection criteria. The zoom insets highlight three regions of interest – namely the mid-latitude mountains of British Columbia, European Alps, and the Greater Caucasus. Each of these mountain ranges receive a large fraction of their precipitation as snow, with some alpine glaciation under modern climate. In these settings (and others), there is a relatively strong correlation between local relief and mean runoff across the study area (Figure 8A-insets), consistent with prior studies (Bookhagen & Burbank, 2006; Bookhagen & Strecker, 2008). The relationship between maximum elevation and snowmelt fraction is more nuanced (Figure 8B-insets). The sign of the correlation depends on whether positioned on the windward or leeward side of prevailing weather systems, whereby windward sides show relatively strong positive correlations. Nevertheless, the most complex of these three regional sites is the Greater Caucasus, where relationships among maximum elevation, snowmelt fraction, and runoff generation has been verified using a finer-scale analysis of gauge records and hydroclimatic data (Forte et al., 2022). Taken as whole, this gives us confidence that these three locations are prime candidates for building regional relationships among topography, snowmelt, and runoff statistics. To develop these local relationships, we consider similar candidate relationships tested on the global scale (Figure 7), specifically mean runoff or snowmelt fraction as a function of either mean elevation, maximum elevation, or local relief (Figure S2).

6 Discussion

6.1 Mean runoff, runoff variability, and snowmelt

The global analysis of WaterGAP3 data helped solidify interpretations that mean runoff and daily runoff variability are inversely correlated. This result was born out both in the Random Forest Regression (Figure 6) and in the individual regressions after binning by snowmelt fraction

(Figures 4-5), thereby supporting findings from prior studies (Molnar et al., 2006; Rossi et al., 2016). The functional form of the relationship between mean runoff and the shape of the daily runoff distribution appears to bifurcate at snowmelt fractions around 0.35 (Figure 5). Below this value, the relationship is highly nonlinear. Above this value, relationships vary but become much more linear. The nonlinearity in rainfall-runoff regimes can be interpreted using ecohydrological models where climatic parameters can exert different relative influences on mean and tail behavior (Deal et al., 2018). The transition to snowmelt hydrology resulting in lower variability flows (e.g., Pitlick, 1994) is expected due to the effects of both increased runoff ratios and the slow release of water from storage. That this transition is abrupt emphasizes the importance of the phase transition from rain to snow in event-scale runoff variability. The snowmelt fractions where this occurs are relatively low suggesting that snowmelt should not be ignored in fluvial erosion models. We also note here that stochastic-threshold models based on stream power were originally developed for small watersheds (e.g., Lague et al., 2005; Tucker, 2004). Given our focus on mountain range scales, it is important to also understand how the spatial footprint of runoff events varies for different runoff generation mechanisms.

To assess the importance of spatial scale to runoff generation, Figure 9 compares the exceedance frequency of the spatial footprints of precipitation and runoff events in the WaterGAP3 data. The area of each ‘event’ is determined by finding spatially contiguous objects in the daily data above a given intensity threshold (i.e., 5 - 35 mm/day). It should be noted that unlike much of the analysis in previous sections, we do not filter by ‘mountainous topography’ (i.e., use elevation or relief to filter the data), and are considering events across all land surfaces. To convert the unprojected pixel-based objects into areas, we multiplied the number of pixels by the size of a pixel in degrees squared. We then calculated the radius of the circle that equals that

area. The radius of the circle is converted from degrees to km in both latitude and longitude. Because the conversion in longitude generally differs from the conversion in latitude, this transformation produces an ellipse with area units of km^2. These are the x-coordinates used for plotting exceedance frequencies (Figure 9A,C,E,G). Furthermore, for runoff data, we labeled each event as snowmelt or rainfall runoff based on the 0.35 snowmelt fraction threshold. Because smaller footprints include both rainfall and snowmelt dominated runoff, the right hand panels (Figure 9B,D,F,H) shows the percent of daily runoff events that are classified as snowmelt for log distributed bins of exceedance frequency. Three important insights emerge from this analysis. First, and unsurprisingly, higher intensity thresholds produce smaller event areas. Second, at around the 25 mm/day threshold, the largest area events in runoff and precipitation (i.e., far right tails) are of similar magnitude. Higher thresholds produce runoff areas larger than comparable frequency precipitation events. Third, the far right tail of the size distribution of runoff is all snowmelt. Taken together, these results suggest that the relative contribution of snowmelt runoff becomes increasingly important for larger watersheds and for increasing intensities.

6.2 Importance of constraining regional relationships

While global relationships linking mean runoff and daily runoff variability via topography were elusive, regional assessment was much more promising. Figure 10 summarizes the kinds of regional rulesets that can be generated from an analysis like ours. At the regional scale, relationships between local relief and mean runoff emerge, consistent with other studies focused on explaining spatial patterns in rainfall (e.g., Bookhagen & Burbank, 2006; Bookhagen & Strecker, 2008). This is thought to arise because high relief corresponds to increased forced lifting of air masses. Local relief (not shown) and maximum elevation (shown) also correlate

with snowmelt fraction likely due to the role of high topography increasing the probability that precipitation will fall in the form of snow. Regardless of mechanisms, our analysis shows the value of producing regionally constrained links between mean runoff and snowmelt fraction via topography. To generate Figure 10, the pixel-based correlation coefficients presented earlier (Figure 8) are summarized into bins of either mean runoff or snowmelt fraction (y-axes). For each bin, the mean and standard deviation of the correlated topographic metric is shown (local relief for mean runoff and maximum elevation for snowmelt fraction). Marker sizes are scaled to the number of observations within a bin. Power law fits for each relationship are shown as lines. In detail, we tested whether better correlations existed between the hydroclimatic variables of interest (mean runoff and snowmelt fraction) and either mean elevation, maximum elevation, and mean local relief (Figure S2). The selected relationships shown in Figure 10, that we also use to parameterize the models in Part 2, were chosen primarily based on either goodness of fit (i.e., which relationships had the lowest root mean squared error) or which ones would be more practical to implement in the models developed in Part 2 when goodness of fit metrics were similar. Each region is described by its own functional relationship, which we interpret as the orographic effects on mean runoff and snowmelt fraction for each mountain range. We suspect that some of the non-monotonic behavior of binned values, especially in snowmelt fraction, are a consequence of mixing windward and leeward components of a regional orographic effect (e.g., Figure 8), as well as along-strike complexity in precipitation sourcing. Nevertheless, summarizing the data in this way allows us to build empirically based rules for mean runoff and snowmelt fraction specific to each region. Together with the observation that the relationship between mean runoff and daily runoff variability abruptly shifts around snowmelt fractions of

715 0.35 allows us to drive a stochastic runoff model using regionally informed parameters from
716 WaterGAP3 in part 2 of this analysis (Forte & Rossi, 2023).

717 The relationships shown in Figure 10 help explain why the role of topography was so
718 hard to extract from the Random Forest Regression (RFR) that included these metrics (Figure 6).
719 First, regional relationships relating topography to runoff generation are quite noisy. While
720 casting runoff parameters as a simple function of topography was our goal, the relatively coarse
721 resolution of water model data, the lack of distinguishing between windward from leeward
722 slopes, and hydro-climatic diversity induced by regional climate will each confound simple
723 relationships between topography and runoff parameters. Second, while the power law functions
724 decently describe snowmelt fraction, the bin-averaged values suggest subtle, non-monotonic
725 relationships with maximum elevation. Third, and perhaps most importantly, the relationship for
726 each regional setting are distinctly different. Any global analysis would struggle to parse this
727 difference.

728 6.3 Implications on landscape evolution studies

729 Two-way coupled models between climate and tectonics require erosion laws for either
730 river incision, glacial erosion, or both. Those testing fluvial dynamics are typically built on the
731 stream power model (e.g., Beaumont et al., 1992; Stolar et al., 2006; Whipple & Meade, 2004;
732 Willett, 1999). Orographic effects in these models focus on the windward ascent and extraction
733 of precipitation. By setting up a contrast in the efficiency of erosion on the windward and
734 leeward sides of mountain ranges, mountain belts adjust their width and height in order to
735 achieve a steady state morphology. The widespread use of stream power in these climate-tectonic
736 models has subsequently motivated many studies to interrogate how orographically induced
737 spatial patterns in precipitation might alter the long-term evolution of river profiles and relief

(Anders et al., 2008; Han et al., 2014; Leonard & Whipple, 2021; Roe et al., 2002, 2003). At the same time, stream power models are increasingly incorporating the role of stochastic streamflow and erosion thresholds to interpret river profiles (DiBiase & Whipple, 2011; Lague, 2014; Lague et al., 2005; Marder & Gallen, 2023; Scherler et al., 2017; Snyder et al., 2003; Tucker, 2004; Tucker & Bras, 2000). The aim in this study was integrate these two productive research threads and explore whether mean runoff, daily runoff variability, and snowmelt fraction can be linked to each other via topographic elevation and relief. As such, we focused our regional analyses on mid-latitude mountain ranges at or near the cusp of glaciation, and where snowmelt contributions to streamflow are significant. While this was our focus, it is worth noting that orographic gradients in stochastic rainfall itself are often poorly constrained. For example, in tropical settings, there can be complex interactions among rainfall type (e.g., convective, monsoonal) that can lead to lower elevation peaks in rainfall maxima (Anders & Nesbitt, 2015) than conventional orographic rules assume, a topic in need of more attention.

Figure 11 is a conceptual diagram illustrating how stochastic runoff parameters might co-evolve with mountain topography in settings where mountain range relief is sufficient to trigger the transition from rainfall-dominated to snowmelt-influence runoff, but where river incision is still setting the relief structure of the landscape (e.g., Whipple et al., 1999). The color coded dots on the schematic mountains in Figure 11A are intended to correspond to the dots on the hypothetical plots relating topography to runoff and snowmelt (Figure 11B) and those relating mean runoff to daily runoff variability (Figure 11C). On the windward side of mountain ranges we expect that the growth of topography will increase mean runoff (Figure 11B solid line) in line with conventional treatments of orographic precipitation (Roe, 2005). This leads to concurrent increases in the frequency of snowfall and thus the snowmelt contribution to runoff (Figure 11B

761 dashed line). While snowmelt fraction has an upper bound of one, in practice, the upper bound
762 we are envisioning in Figure 11B will be less than one because rain continues to fall at lower
763 elevations and because the temperatures required to enhance very high snowmelt fractions would
764 also entail a transition to glaciation. The key behavior in this conceptual framework is that
765 accounting for snowmelt dynamics leads to a markedly different relationship between mean
766 runoff and the shape parameter of the daily runoff distribution (Figure 11C). Our global analysis
767 of WaterGAP3 data suggests that this transition might be abrupt. We identified a snowmelt
768 fraction of ~0.35 corresponds to this transition, with the important caveat that this is based on a
769 water model dataset that tends to produce underestimates of the shape parameter (Figure 3B).
770 Furthermore, while the bulk of the data supports the notion that this transition is relatively
771 abrupt, there are a number of exceptions to this pattern in both the water model and observational
772 data (Figures 1B; 4; 5A). These exceptions may be due uncertainty in the proposed snowmelt
773 transition or evidence for the numerous other hydrological considerations that can reduce daily
774 variability in rainfall-dominated regimes (e.g., seasonality, groundwater, drainage basin size).
775 Regardless, the global analysis reveals that the strength and form of these relationships need to
776 be assessed independently for any given mountain range (Figure 10). However, by simplifying
777 the hydrology into just two parameters, these kinds of relationships are well-suited to driving
778 long term models of river incision (e.g., Lague et al., 2005; Tucker, 2004) in ways that can be
779 linked to mean climate (DiBiase & Whipple, 2011) and ecohydrology (Deal et al., 2018).

780 While we think there is observational evidence for these dynamics in actual landscapes
781 (Forte et al., 2022), we highlight a few important caveats to generalizing from our large-scale
782 analysis of the WaterGAP3 water model data. First, this conceptual model is better suited to
783 explaining the windward side of mountain ranges where precipitation, and thus runoff, is

enhanced by topography. To build better rulesets, higher resolution runoff datasets that honor physiographic transitions and water divides are likely needed. Second, this conceptual model requires that mean runoff and rare runoff events are linked via some common mechanism. This need not be the case. For example, recent work in the Colorado Front Range showed how mean runoff was largely driven by snowmelt throughout the landscape while daily runoff variability was driven by rainfall runoff at lower elevations in response to thinning soils (Rossi et al., 2020). Such mechanistic controls on mean runoff and daily runoff variability are at play in all landscapes and may partially explain the wide variance of runoff parameters observed in our regional rulesets (Figure 10). Third, statistical analyses all assumed independence of daily runoff events which is decidedly not true as runoff events, especially large ones, can extend over multiple days (synoptic-scale storms) to seasons (snowmelt, monsoons). Despite these caveats, this analysis produced empirically-based runoff parameters that vary in space and time. As such, this provides the minimal constraints needed to integrate orographic effects with stochastic runoff generation for river profile modeling (Forte & Rossi, 2023).

7. Conclusions

The results of our global analysis of WaterGAP3 data largely confirm, and significantly expand upon, past results indicating a negative correlation between mean runoff and daily runoff variability. The form of the relationship between variability and mean runoff is linked to the fraction of runoff from snowmelt. For snowmelt fractions <0.35, mean runoff and variability are related via a power law. At higher snowmelt fractions, the two are linearly related. We also find that snowmelt produces runoff events with a much larger areal extent than rainfall runoff.

Exploration of the extent to which mean runoff, runoff variability, and snowmelt fraction are related to topography produces ambiguous results at the global scale. Unsupervised machine

learning methods highlight that simple topographic variables such as mean elevation, maximum elevation, and local relief do not have strong predictive power for our target hydroclimatological parameters of mean runoff, snowmelt fraction, and daily runoff variability. Attempts to identify cross-correlations that may be masking the role of topography were more suggestive, but still difficult to interpret. Results from the global analysis emphasize that exploring relationships between topography and hydroclimatology requires a regional approach. For three mid-latitude mountain ranges - the European Alps, Greater Caucasus, and southern British Columbia – we find robust positive relationships between mean runoff and mean local relief and snowmelt fraction and maximum elevation.

The links between topography, mean runoff, daily runoff variability, and snowmelt fraction highlight that multiple aspects of hydroclimate of mountain ranges should be expected to evolve as topography grows. Past work on this topic has primarily focused on the influence of growing topography on the development of orographic patterns in rainfall. When coupled to tectonic models and simple hydrologic models equating patterns in mean rainfall to mean runoff, orographic effects have been shown to drive a variety of feedbacks between surface processes and tectonics. Our results show how to move beyond mean precipitation or mean runoff when considering the coupled evolution of topography, tectonics, and climate. Both snowmelt fraction and mean runoff are expected to increase with growing topography and reduce daily runoff variability, emphasizing the need to explicitly consider snowmelt dynamics in coupled tectonic – landscape evolution models.

Acknowledgments

Support for M.W. Rossi came from the Geomorphology and Land-use Dynamics (GLD) Program (EAR-1822062). Neither AMF or MWR have any real or perceived financial or other

conflicts with the contents of this work. We thank Mikael Attal for editorial handling and also Associate Editor Liran Goren and reviewers Alison Anders, Eric Deal, and an anonymous reviewer for their comments that improved this manuscript.

Open Research

Analysis codes necessary to reproduce this work are available in Forte (2024). Larger outputs of the processing steps are available in Forte & Rossi (2024). Portions of these analysis codes rely on publicly available datasets that we do not have permission to redistribute, but when used, we provide comments in the code referencing where these datasets can be downloaded.

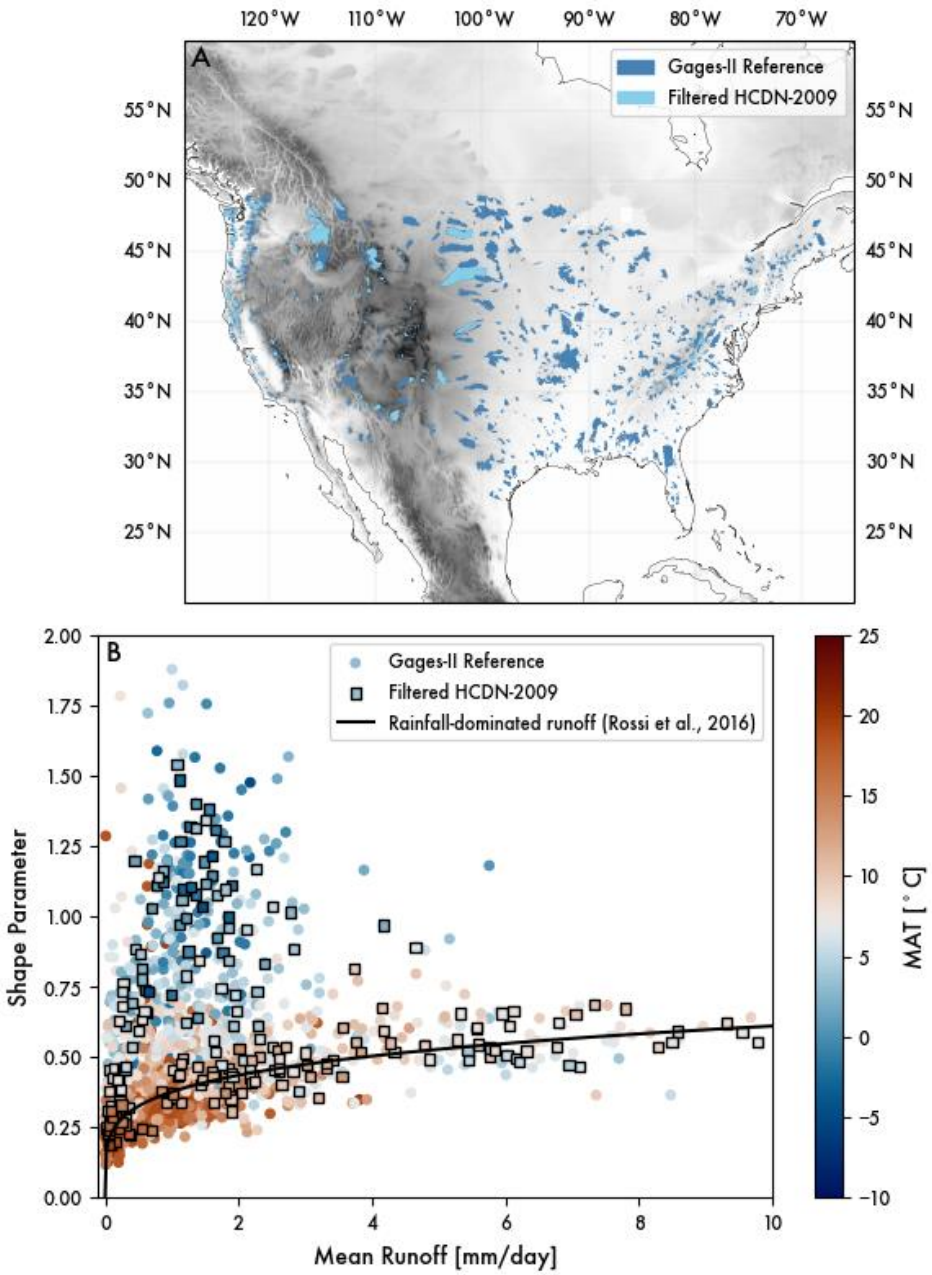

840

841 **Figure 1.** Observational stream gauge data used in this study includes (A) gauged sites in the
842 contiguous United States that are minimally impacted by human management, which are then
843 used to characterize (B) the relationship between mean runoff and the shape parameters
844 describing daily runoff distributions for each stream gauge. In A, a subset of the reference
845 stations in the GAGES-II network were used for the water model validation presented below

(i.e., filtered HCDN-2009). In B, two broad trends between mean runoff and daily runoff variability organize around mean annual temperature, which prior authors have interpreted as reflecting the transition from snowmelt-dominated to rainfall-dominated systems (Rossi et al., 2016).

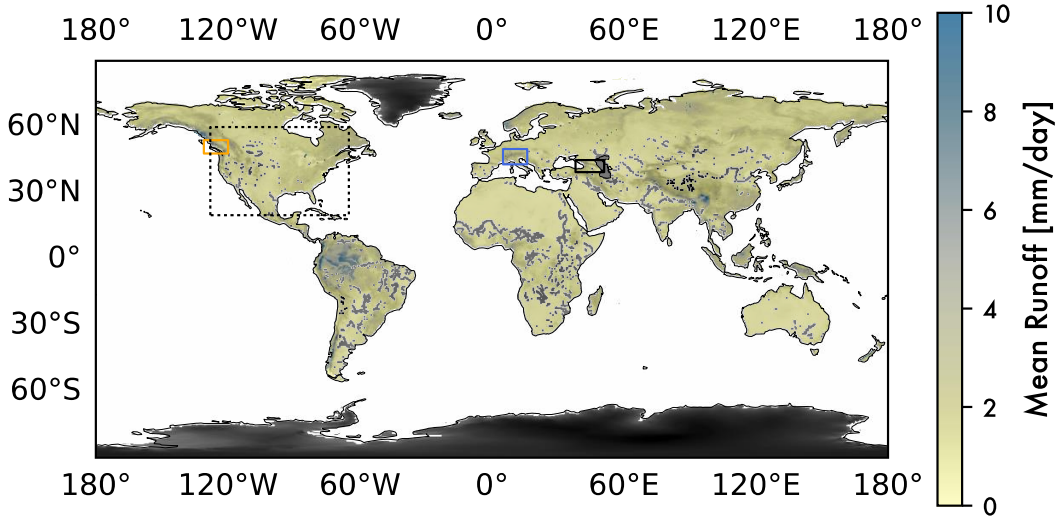

Figure 2. Global mean runoff from the WaterGAP3 water model (1980-1999). The dotted black box corresponds to the area shown in Figure 1A and bounds the geographic extent of the validation data used. The three smaller colored boxes show the geographic extent of the three mid-latitude, regional case studies introduced in section 4.4.

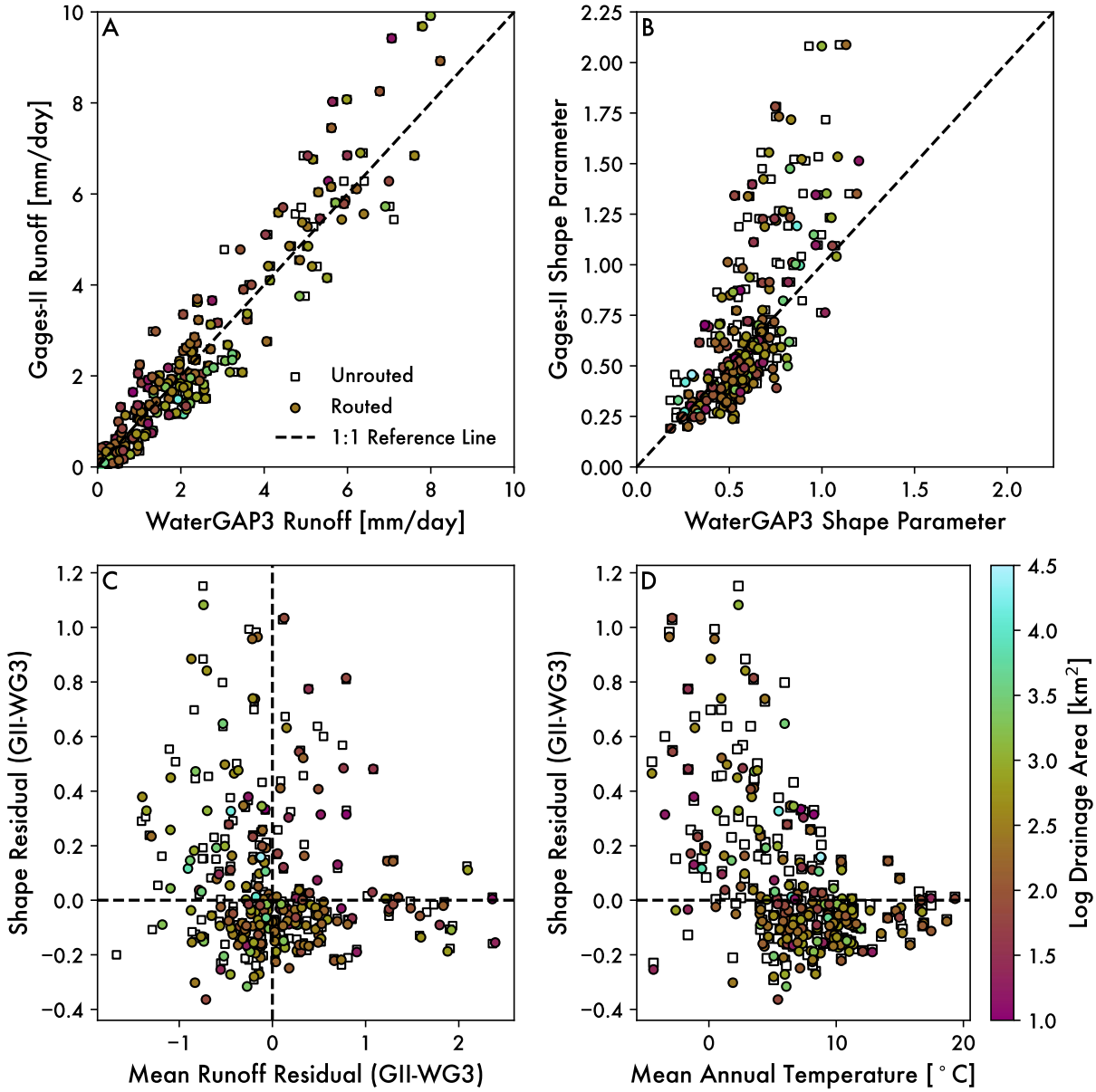

856

857 **Figure 3**. Comparison of WaterGAP3 runoff parameters against selected HCDN-2009 stream
858 gage data, colored by the log of the drainage area of individual gaged basins: (A) Mean runoff
859 values, (B) Shape parameters of daily distributions, (C) Mean and shape residuals with respect to
860 1:1 line, and (D) Shape residuals against mean annual temperatures for each watershed. Open
861 squares are arithmetic means of WaterGAP3 values within watershed boundaries. Closed and
862 colored circles route daily WaterGAP3 data to generate a time series that is then used to calculate

fit parameters. Dashed lines in the upper panels indicate the 1:1 relationship between the water model and gaged data whereas dashed lines in the lower panels reflect a 0 residual value.

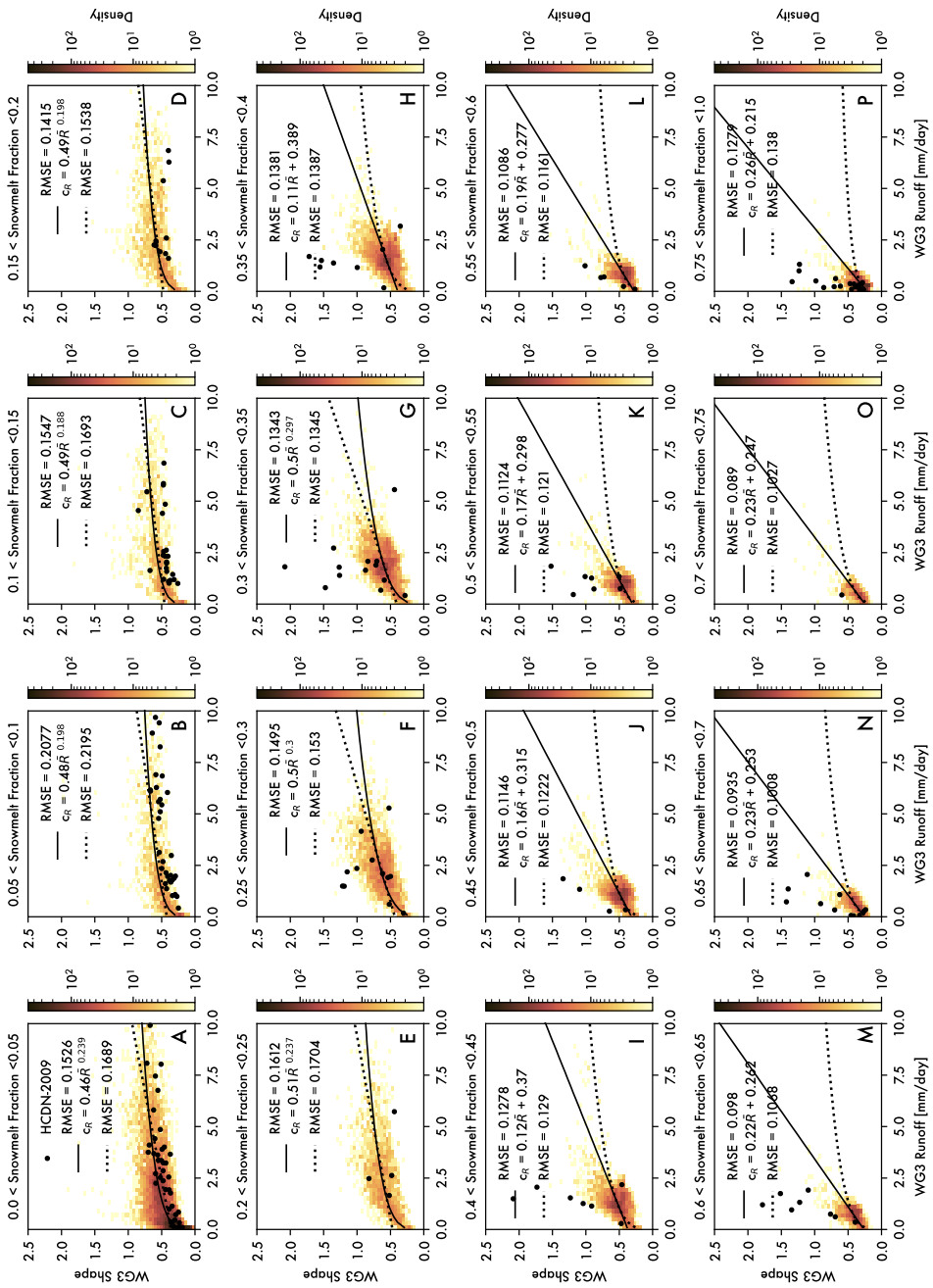

Figure 4. Density plots show the relationship between the shape parameter and mean runoff for the filtered WaterGAP3 data: (A-O) Plots binned by snowmelt fraction in increments of 0.05 up

868 to 0.75 snowmelt. (P) The last panel is for the remaining data that has >0.75 snowmelt. In all
869 panels, both a power law and linear fit are shown. The better fit is shown using a solid line and is
870 based on having a lower RMSE. Results are the same if using the reduced chi squared statistic.

871 Black dots are HCDN-2009 watersheds filtered in the same way. For HCDN-2009 data,
872 snowmelt fraction was taken from WaterGAP3 data.

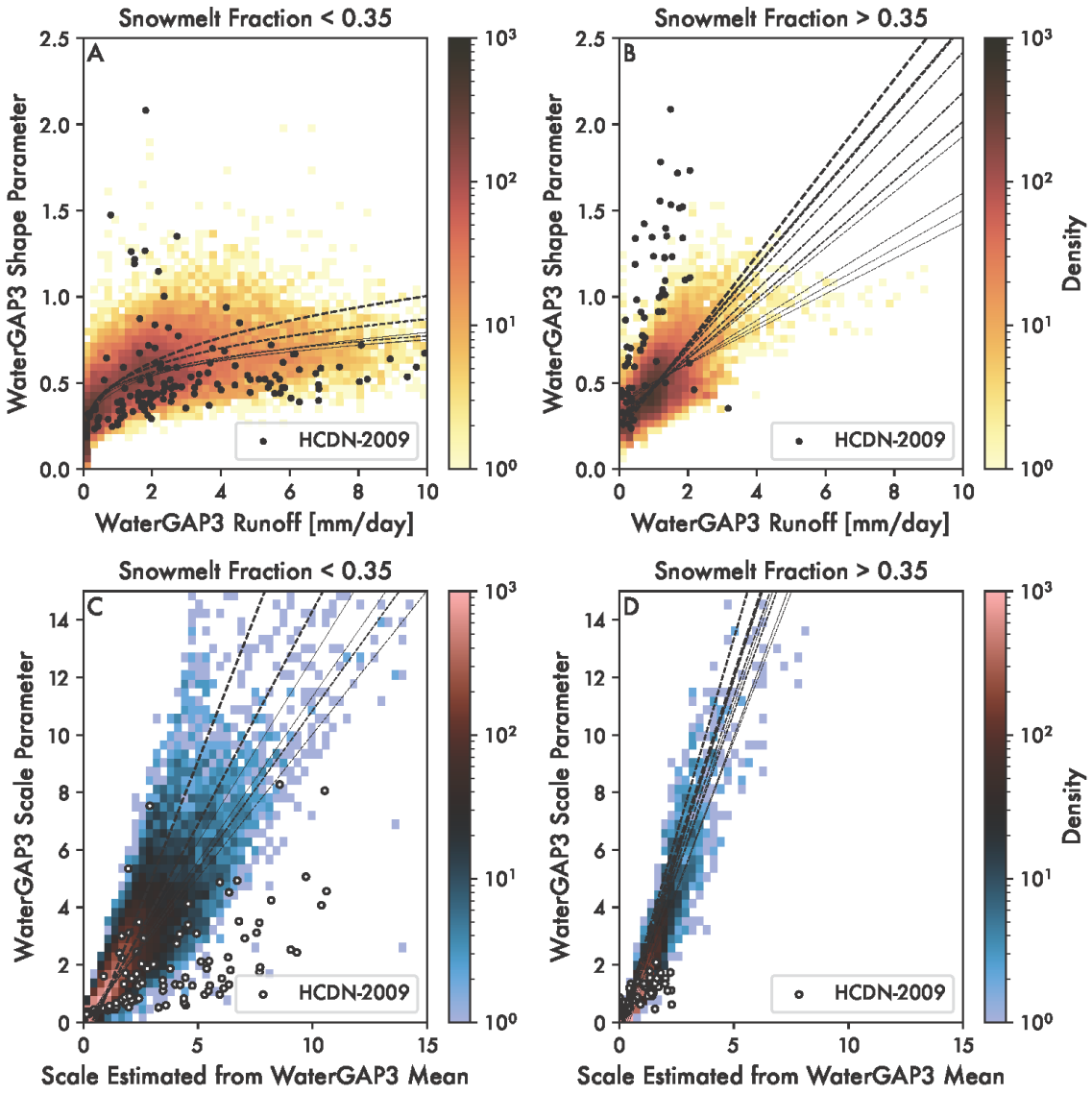

873

874 **Figure 5.** Density plots showing relationships among the scale and shape parameters of
875 parametric fits with the mean runoff observed for the filtered WaterGAP3 data. (A) Relationship
876 between mean runoff and shape of the right tail for pixels where snowmelt fraction is <0.35. (B)
877 Relationship between mean runoff and shape of the right tail for pixels where snowmelt fraction

878 is >0.35. Because parametric fits include a threshold, the mean of the distribution cannot be
879 directly inferred from scale parameters. (C) Relationship between the scale parameters fit to the
880 data versus those implied from the empirical mean for pixels where snowmelt fraction is <0.35.
881 (D) Relationship between the scale parameters fit to the data versus those implied from the
882 empirical mean for pixels where snowmelt fraction is >0.35.Black dots are HCDN-2009
883 watersheds filtered in the same way. The strongest regressions from Figure 4 (A-B) and Figure
884 S1 (C-D) subpanels are shown for reference.

885

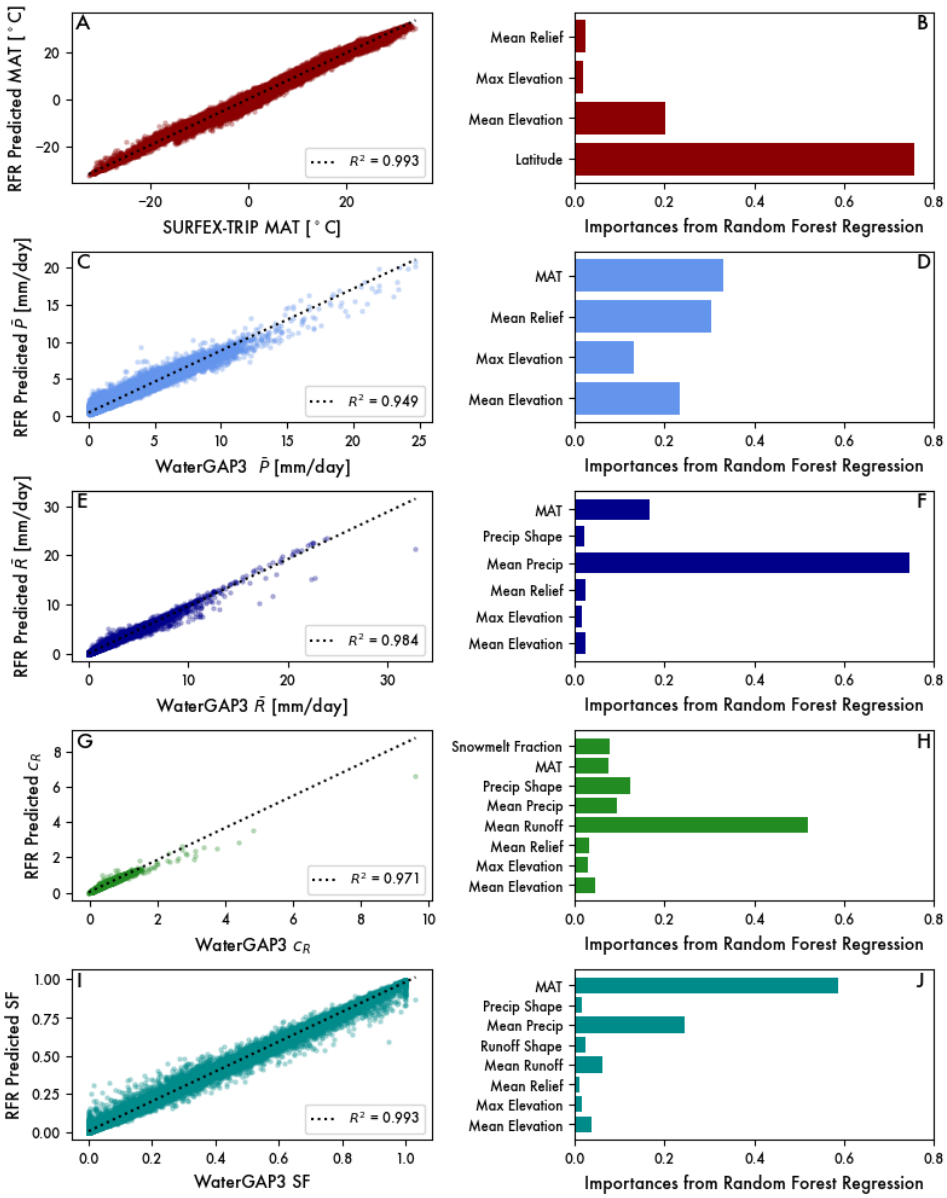

Figure 6. Results from the random forest regression for predicting: (A-B) Mean Temperature, (C-D) Mean Precipitation, (E-F) Mean Runoff, (G-H) Runoff Variability, and (I-J) Snowmelt

Fraction. For each target variable, the left plot compares observed versus predicted data (linear fit with R^2 shown for reference), and the right plot shows the relative importance of predictors.

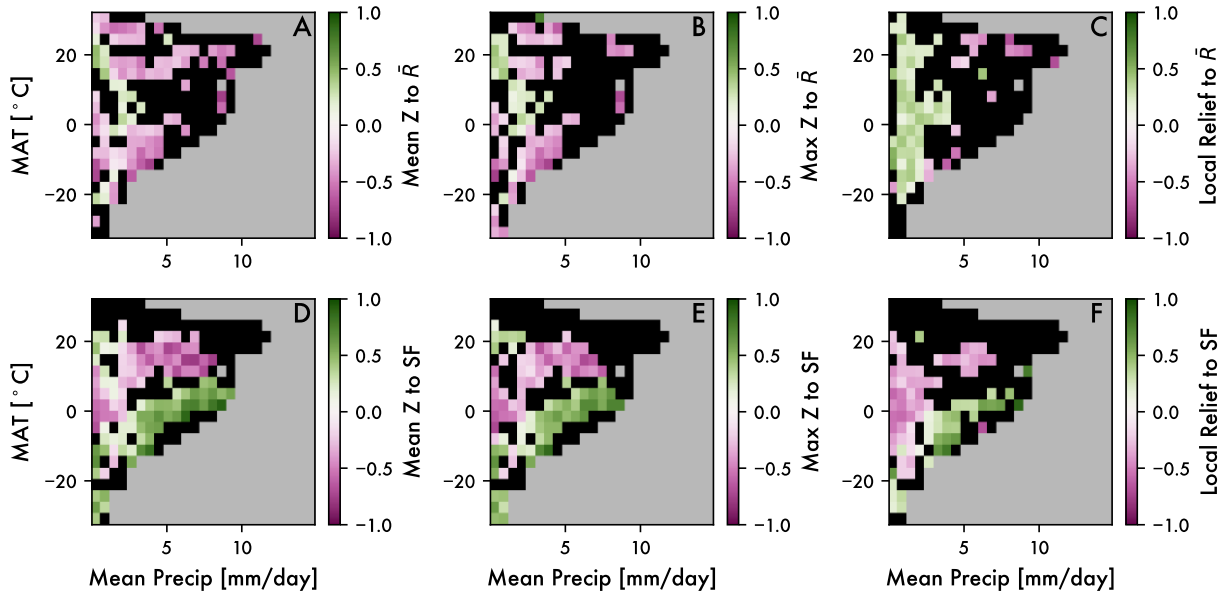

Figure 7. Spearman's rank correlation coefficients within temperature-precipitation bins. (A-C) Coefficients relating topography and mean runoff. (D-F) Coefficients relating topography to snowmelt fraction. The topographic variables considered were mean elevation (A, D), maximum elevation (B, E), and local relief (C, F). For all plots, the gray area indicates regions of parameter space with less than 10 observations. Black regions indicate there were greater than 10 observations, but that the correlation did not exceed the 95% confidence interval. Note that these plots obscure the number of observations in each precipitation – temperature bin. As such, see Figure 8 to assess the distribution of correlations coefficient within their spatial context.

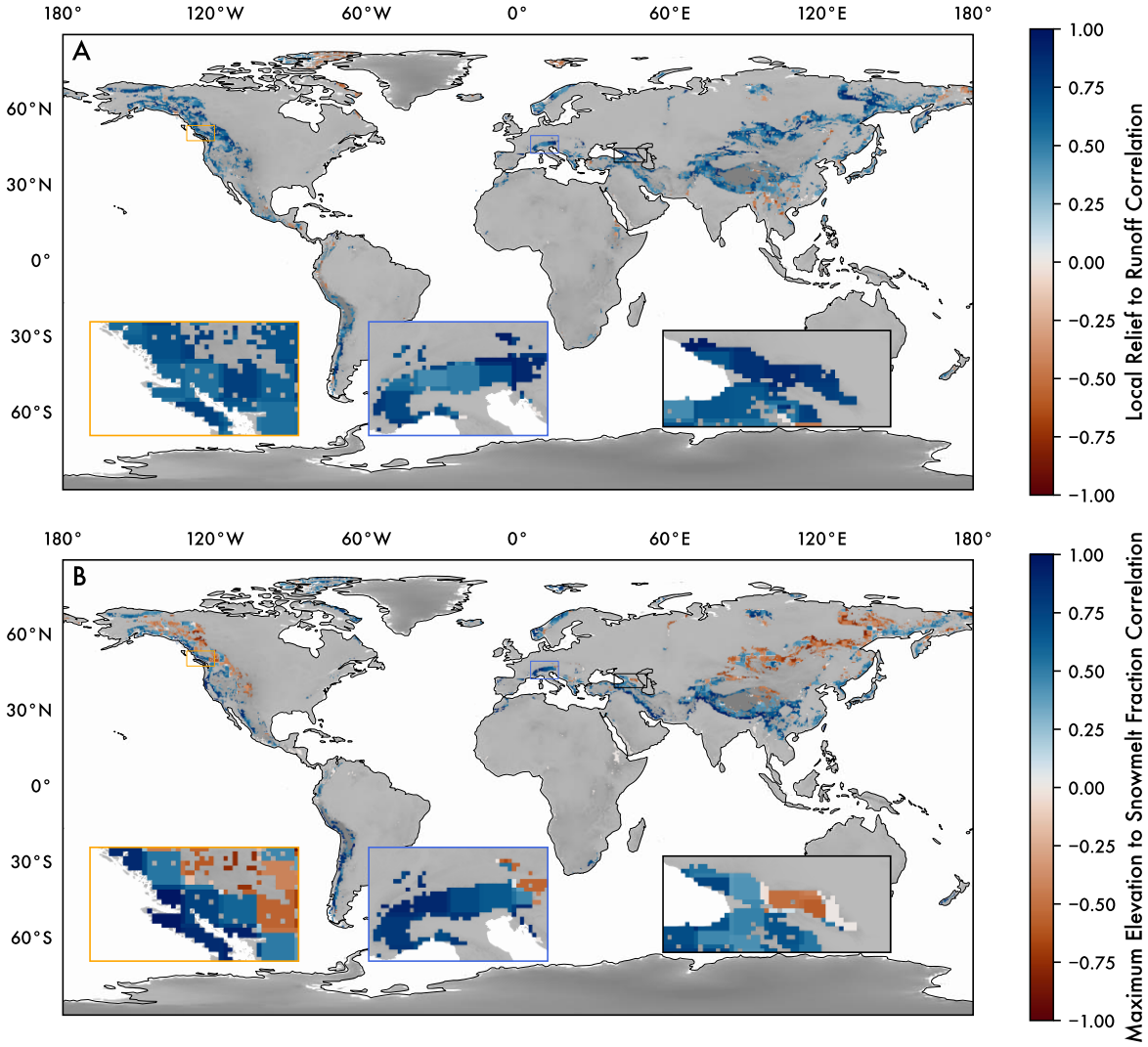

903

904 **Figure 8.** Relationships among topography, mean runoff, and snowmelt fraction in map view.
905 (A) Mean spearman rank correlation coefficient within a 2° moving window for mean runoff and
906 local relief. (B) Mean spearman rank correlation coefficient within a 2° moving window for
907 maximum elevation and snowmelt fraction. After filtering the WaterGAP3 data for mountain
908 settings (see text for details), only a small area remains. Insets highlight results for the three
909 regional cases considered.

910

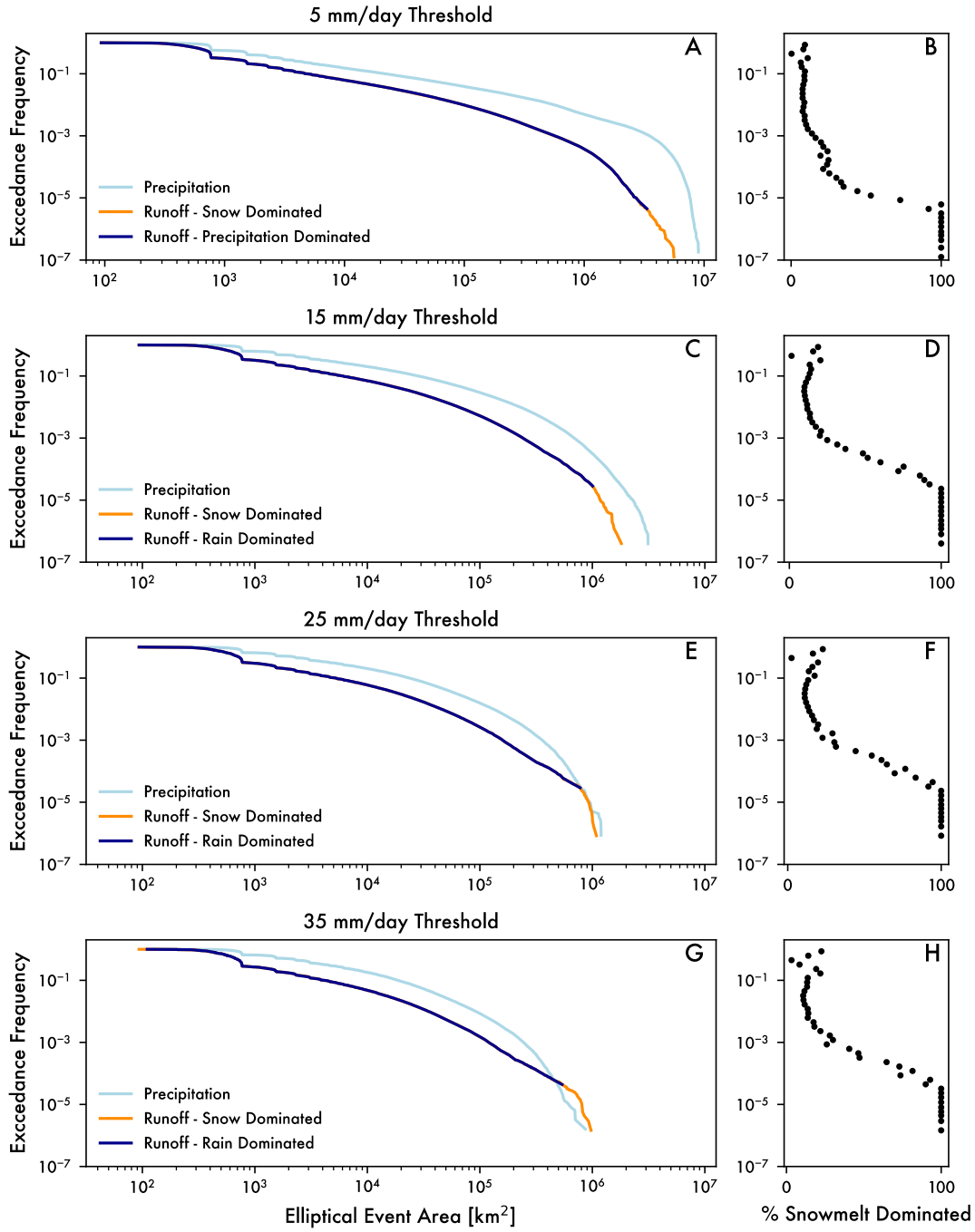

Figure 9. Exceedance probability distributions of daily event sizes of different magnitudes: (A-B) 5 mm/day, (C-D) 15 mm/day, (E-F) 25 mm/day, and (G-H) 35 mm/day. The left panels show probability plots for both precipitation and runoff, whereby the latter is color-coded by runoff generation source. After classifying runoff events in this way, the right panels show what

916 fraction of events are snowmelt dominated within exceedance probability bins. Note that
917 regardless of intensity threshold the largest area runoff events are snowmelt dominated. At
918 higher intensity thresholds, these event sizes can exceed the largest area precipitation events.

919

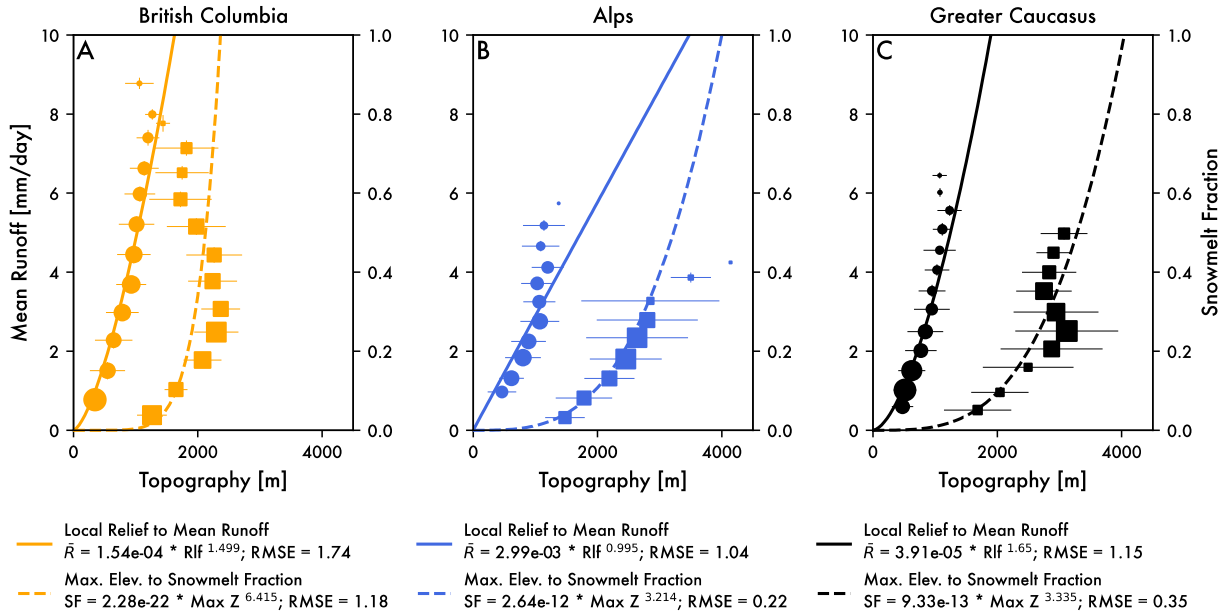

920

921 **Figure 10.** Relationships among topography, mean runoff, and snowmelt fraction for the three
922 regional cases (see Figure 8 for locations): (A) British Columbia, (B) European Alps, and (C)
923 Greater Caucasus. In all three plots, circles are binned mean runoff to local relief, and squares
924 are binned snowmelt fraction to maximum elevation. Symbols are scaled to number of
925 observations in the bin and whiskers show one standard deviation. Power law fits for binned data
926 relate local relief and mean runoff (solid line) and maximum elevation and snowmelt fraction
927 (dashed line). In all three panels, the "Topography" x-axis plots both local relief (solid line) and

maximum elevation (dashed line). These fits serve as the basis for orographic rules used in our complementary model study (Forte & Rossi, 2023).

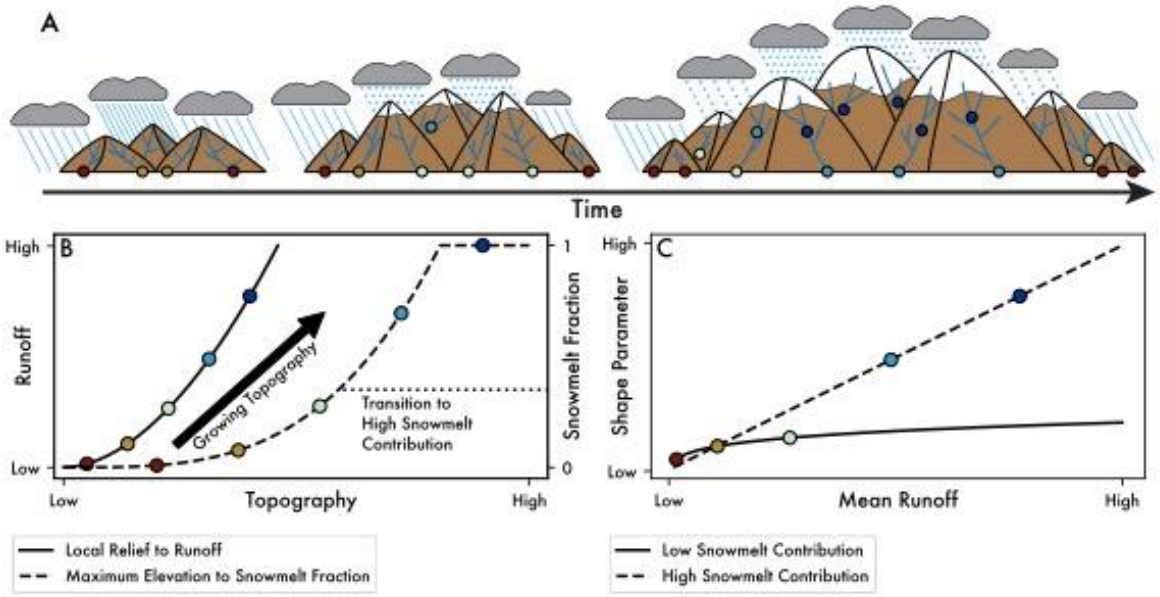

Figure 11. Conceptual model for how orographic controls on runoff variability can be represented in a landscape evolution model. (A) Cartoon showing how precipitation and runoff generation mechanisms might change as a mountain range grows. (B) Example rules for how topography is translated into more runoff and a larger snowmelt fraction as topography grows. (C) Relationship between mean runoff and daily runoff variability in response to those rules. In B, the example ruleset shows that as mountain topography grows, increasing relief leads to more runoff generation on the windward side of a mountain range and increasing elevations lead to a higher fraction of snowmelt. In C, these topography-runoff relationships translate into a much different relationship between mean runoff and daily runoff variability that encodes the transition from rainfall- to snowmelt-dominated runoff events.

References

Adam, J. C., Hamlet, A. F., & Lettenmaier, D. P. (2009). Implications of global climate change for snowmelt hydrology in the twenty-first century. *Hydrological Processes*, *23*(7), 962–972. https://doi.org/10.1002/hyp.7201

Adams, B. A., Whipple, K. X., Forte, A. M., Heimsath, A. M., & Hodges, K. V. (2020). Climate controls on erosion in tectonically active landscapes. *Science Advances*, *6*(42). https://doi.org/10.1126/sciadv.aaz3166

Alcamo, J., Döll, P., Henrichs, T., Kaspar, F., Lehner, B., Rösch, T., & Siebert, S. (2003). Development and testing of the WaterGAP 2 global model of water use and availability. *Hydrological Sciences Journal*, *48*(3), 317–337. https://doi.org/10.1623/hysj.48.3.317.45290

Anders, A. M., & Nesbitt, S. W. (2015). Altitudinal Precipitation Gradients in the Tropics from Tropical Rainfall Measuring Mission (TRMM) Precipitation Radar. *Journal of Hydrometeorology*, *16*(1), 441–448. https://doi.org/10.1175/JHM-D-14-0178.1

Anders, A. M., Roe, G. H., Montgomery, D. R., & Hallet, B. (2008). Influence of precipitation phase on the form of mountain ranges. *Geology*, *36*(6), 479. https://doi.org/10.1130/G24821A.1

Barnett, T. P., Adam, J. C., & Lettenmaier, D. P. (2005). Potential impacts of a warming climate on water availability in snow-dominated regions. *Nature*, *438*(7066), 303–309. https://doi.org/10.1038/nature04141

Barnhart, T. B., Molotch, N. P., Livneh, B., Harpold, A. A., Knowles, J. F., & Schneider, D. (2016). Snowmelt rate dictates streamflow. *Geophysical Research Letters*, *43*(15), 8006–8016. https://doi.org/10.1002/2016GL069690

Barros, A. P., & Lettenmaier, D. P. (1994). Dynamic modeling of orographically induced precipitation. *Reviews of Geophysics*, *32*(3), 265. https://doi.org/10.1029/94RG00625

Basso, S., Merz, R., Tarasova, L., & Miniussi, A. (2023). Extreme flooding controlled by stream network organization and flow regime. *Nature Geoscience*, *16*(4), 339–343. https://doi.org/10.1038/s41561-023-01155-w

Beaumont, C., Fullsack, P., & Hamilton, J. (1992). Erosional control of active compressional orogens. In K. R. McClay (Ed.), *Thrust Tectonics* (pp. 1–18). New York: Chapman Hall.

969 Beck, H. E., van Dijk, A. I. J. M., de Roo, A., Dutra, E., Fink, G., Orth, R., & Schellekens, J. (2017). Global
970 evaluation of runoff from 10 state-of-the-art hydrological models. *Hydrology and Earth System Sciences*,
971 *21*(6), 2881–2903. https://doi.org/10.5194/hess-21-2881-2017
972 Berghuijs, W. R., Woods, R. A., & Hrachowitz, M. (2014). A precipitation shift from snow towards rain leads to a
973 decrease in streamflow. *Nature Climate Change*, *4*(7), 583–586. https://doi.org/10.1038/nclimate2246
974 Berghuijs, W. R., Harrigan, S., Molnar, P., Slater, L. J., & Kirchner, J. W. (2019). The Relative Importance of
975 Different Flood-Generating Mechanisms Across Europe. *Water Resources Research*, *55*(6), 4582–4593.
976 https://doi.org/10.1029/2019WR024841
977 Bookhagen, B., & Burbank, D. (2006). Topography, relief, and TRMM-derived rainfall variations along the
978 Himalaya. *Geophysical Research Letters*, *33*, L08405–L08405. https://doi.org/10.1029/2006GL026037
979 Bookhagen, B., & Burbank, D. (2010). Toward a complete Himalayan hydrological budget: Spatiotemporal
980 distribution of snowmelt and rainfall and their impact on river discharge. *Journal of Geophysical Research*,
981 *115*(F03019). https://doi.org/10.01029/02009JF001426
982 Bookhagen, B., & Strecker, M. R. (2008). Orographic barriers, high-resolution TRMM rainfall, and relief variations
983 in the eastern Andes. *Geophysical Research Letters*, *35*(L06403). https://doi.org/10.1029/2007GL032011
984 Bookhagen, B., & Strecker, M. R. (2011). Modern Andean Rainfall Variation during ENSO Cycles and its Impact
985 on the Amazon Drainage Basin. In C. Hoorn & F. P. Wesselingh (Eds.), *Amazonia: Landscape and Species*
986 *Evolution* (pp. 223–241). Oxford, UK: Wiley-Blackwell Publishing Ltd.
987 https://doi.org/10.1002/9781444306408.ch14
988 Botter, G., Porporato, A., Rodriguez-Iturbe, I., & Rinaldo, A. (2009). Nonlinear storage-discharge relations and
989 catchment streamflow regimes: STREAMFLOW REGIMES OF NONLINEAR CATCHMENT. *Water*
990 *Resources Research*, *45*(10). https://doi.org/10.1029/2008WR007658
991 Campforts, B., Vanacker, V., Herman, F., Vanmaercke, M., Schwanghart, W., Tenorio, G. E., et al. (2020).
992 Parameterization of river incision models requires accounting for environmental heterogeneity: insights
993 from the tropical Andes. *Earth Surface Dynamics*, *8*(2), 447–470. https://doi.org/10.5194/esurf-8-447-2020
994 Crave, A., & Davy, P. (2001). A stochastic "precipiton" model for simulating erosion/sedimentation dynamics.
995 *Computers & Geosciences*, *27*(7), 815–827. https://doi.org/10.1016/S0098-3004(00)00167-9

996 Deal, E., Favre, A. C., & Braun, J. (2017). Rainfall variability in the Himalayan orogen and its relevance to erosion
997 processes. *Water Resources Research*, *53*(5), 4004–4021. https://doi.org/10.1002/2016WR020030
998 Deal, E., Braun, J., & Botter, G. (2018). Understanding the Role of Rainfall and Hydrology in Determining Fluvial
999 Erosion Efficiency. *Journal of Geophysical Research: Earth Surface*, *123*(4), 744–778.
1000 https://doi.org/10.1002/2017JF004393
1001 Decharme, B., Alkama, R., Douville, H., Becker, M., & Cazenave, A. (2010). Global Evaluation of the ISBA-TRIP
1002 Continental Hydrological System. Part II: Uncertainties in River Routing Simulation Related to Flow
1003 Velocity and Groundwater Storage. *Journal of Hydrometeorology*, *11*(3), 601–617.
1004 https://doi.org/10.1175/2010JHM1212.1
1005 Decharme, B., Martin, E., & Faroux, S. (2013). Reconciling soil thermal and hydrological lower boundary
1006 conditions in land surface models: LOWER BOUNDARY CONDITIONS OF SOIL IN LSM. *Journal of*
1007 *Geophysical Research: Atmospheres*, *118*(14), 7819–7834. https://doi.org/10.1002/jgrd.50631
1008 Desormeaux, C., Godard, V., Lague, D., Duclaux, G., Fleury, J., Benedetti, L., et al. (2022). Investigation of
1009 stochastic-threshold incision models across a climatic and morphological gradient. *Earth Surface*
1010 *Dynamics*, *10*(3), 473–492. https://doi.org/10.5194/esurf-10-473-2022
1011 DiBiase, R. A., & Whipple, K. X. (2011). The influence of erosion thresholds and runoff variability on the
1012 relationships among topography, climate, and erosion rate. *Journal of Geophysical Research*, *116*(F04036).
1013 https://doi.org/10.1029/2011JF002095
1014 DiBiase, R. A., Whipple, K. X., Heimsath, A. M., & Ouimet, W. B. (2010). Landscape form and millennial erosion
1015 rates in the San Gabriel Mountains, CA. *Earth and Planetary Science Letters*, *289*(1–2), 134–144.
1016 Doane, D. P. (1976). Aesthetic Frequency Classifications. *The American Statistician*, *30*(4). Retrieved from
1017 https://amstat.tandfonline.com/doi/abs/10.1080/00031305.1976.10479172
1018 Döll, P., Kaspar, F., & Lehner, B. (2003). A global hydrological model for deriving water availability indicators:
1019 model tuning and validation. *Journal of Hydrology*, *270*(1–2), 105–134. https://doi.org/10.1016/S0022-
1020 1694(02)00283-4
1021 Dupuis, D. J. (1998). Exceedances over High Thresholds: A Guide to Threshold Selection. *Extremes*, *1*(3), 251–261.

1022 Eagleson, P. S. (1978). Climate, soil, and vegetation: 2. The distribution of annual precipitation derived from
1023 observed storm sequences. *Water Resources Research*, *14*(5), 713–721.
1024 https://doi.org/10.1029/WR014i005p00713
1025 Eisner, S. (2015). *Comprehensive evaluation of the waterGAP3 model across climatic, physiographic, and*
1026 *anthropogenic gradients*. University of Kassel.
1027 Falcone, J. A. (2011). *GAGES-II: Geospatial Attributes of Gages for Evaluating Streamflow* (Report). Reston, VA.
1028 https://doi.org/10.3133/70046617
1029 Farr, T. G., Rosen, P. A., Caro, E., Crippen, R., Duren, R., Hensley, S., et al. (2007). The shuttle radar topography
1030 mission. *Reviews of Geophysics*, *45*, 1–33.
1031 Fatichi, S., Vivoni, E. R., Ogden, F. L., Ivanov, V. Y., Mirus, B., Gochis, D., et al. (2016). An overview of current
1032 applications, challenges, and future trends in distributed process-based models in hydrology. *Journal of*
1033 *Hydrology*, *537*, 45–60. https://doi.org/10.1016/j.jhydrol.2016.03.026
1034 Forte, A. M. (2024, January). amforte/snowmelt_orography: Snowmelt Orography (Version v2.0). Zenodo.
1035 https://doi.org/10.5281/zenodo.10449397
1036 Forte, A. M., & Rossi, M. W. (2023). Stochastic in Space and Time: Part 2, Effects of Simulating Orographic
1037 Gradients in Daily Runoff Variability on Bedrock River Incision. ESSOAr.
1038 https://doi.org/10.22541/essoar.168882084.46051822/v1
1039 Forte, A. M., & Rossi, M. W. (2024). Data and Model Results Associated with Stochastic in Space and Time: Parts
1040 1 and 2. (Version 2.0) [Data set]. https://doi.org/10.5281/zenodo.10407347
1041 Forte, A. M., Whipple, K. X., Bookhagen, B., & Rossi, M. W. (2016). Decoupling of modern shortening rates,
1042 climate, and topography in the Caucasus. *Earth and Planetary Science Letters*, *449*, 282–294.
1043 https://doi.org/10.1016/j.epsl.2016.06.013
1044 Forte, A. M., Leonard, J. S., Rossi, M. W., Whipple, K. X., Heimsath, A. M., Sukhishvili, L., et al. (2022). Low
1045 variability runoff inhibits coupling of climate, tectonics, and topography in the Greater Caucasus. *Earth*
1046 *and Planetary Science Letters*, *584*. https://doi.org/10.1016/j.epsl.2022.117525
1047 Galewsky, J. (2009). Rain shadow development during the growth of mountain ranges: An atmospheric dynamics
1048 perspective. *Journal of Geophysical Research*, *114*(F1), F01018. https://doi.org/10.1029/2008JF001085

1049 Grömping, U. (2009). Variable Importance Assessment in Regression: Linear Regression versus Random Forest.
1050 *The American Statistician*, *63*(4), 308–319. https://doi.org/10.1198/tast.2009.08199
1051 Han, J., Gasparini, N. M., Johnson, J. P. L., & Murphy, B. P. (2014). Modeling the influence of rainfall gradients on
1052 discharge, bedrock erodibility, and river profile evolution, with application to the Big Island, Hawai'i.
1053 *Journal of Geophysical Research*, *119*, 1418–1440. https://doi.org/10.1002/203JF002961
1054 Harel, M. A., Mudd, S. M., & Attal, M. (2016). Global analysis of the stream power law parameters based on
1055 worldwide 10Be denudation rates. *Geomorphology*, *268*, 184–196.
1056 https://doi.org/10.1016/j.geomorph.2016.05.035
1057 Howard, A. D. (1994). A detachment-limited model of drainage basin evolution. *Water Resources Research*, *30*(7),
1058 2261–2285.
1059 Huang, X., & Niemann, J. D. (2006). An evaluation of the geomorphically effective event for fluvial processes over
1060 long periods: GEOMORPHICALLY EFFECTIVE EVENT. *Journal of Geophysical Research: Earth*
1061 *Surface*, *111*(F3), n/a-n/a. https://doi.org/10.1029/2006JF000477
1062 Jiang, Q. (2003). Moist dynamics and orographic precipitation. *Tellus A: Dynamic Meteorology and Oceanography*,
1063 *55*(4), 301. https://doi.org/10.3402/tellusa.v55i4.14577
1064 Kirby, E., & Whipple, K. X. (2012). Expression of active tectonics in erosional landscapes. *Journal of Structural*
1065 *Geology*, *44*, 54–75.
1066 Kirchner, J. W. (2009). Catchments as simple dynamical systems: Catchment characterization, rainfall-runoff
1067 modeling, and doing hydrology backward: CATCHMENTS AS SIMPLE DYNAMICAL SYSTEMS.
1068 *Water Resources Research*, *45*(2). https://doi.org/10.1029/2008WR006912
1069 Lague, D. (2014). The stream power river incision model: evidence, theory and beyond. *Earth Surface Processes*
1070 *and Landforms*, *39*(1), 38–61. https://doi.org/10.1002/esp.3462
1071 Lague, D., Hovius, N., & Davy, P. (2005). Discharge, discharge variability, and the bedrock channel profile. *Journal*
1072 *of Geophysical Research*, *110*, F04006–F04006. https://doi.org/10.1029/2004JF000259
1073 Laherrère, J., & Sornette, D. (1998). Stretched exponential distributions in nature and economy: "fat tails" with
1074 characteristic scales. *The European Physical Journal B*, *2*(4), 525–539.
1075 https://doi.org/10.1007/s100510050276

1076 Lehner, B., Verdin, K., & Jarvis, A. (2008). New Global Hydrography Derived From Spaceborne Elevation Data.
1077 *Eos, Transactions American Geophysical Union*, *89*(10), 93. https://doi.org/10.1029/2008EO100001
1078 Leonard, J. S., & Whipple, K. X. (2021). Influence of Spatial Rainfall Gradients on River Longitudinal Profiles and
1079 the Topographic Expression of Spatially and Temporally Variable Climates in Mountain Landscapes.
1080 *Journal of Geophysical Research: Earth Surface*, *126*(12). https://doi.org/10.1029/2021JF006183
1081 Leonard, J. S., Whipple, K. X., & Heimsath, A. M. (2023). Isolating climatic, tectonic, and lithologic controls on
1082 mountain landscape evolution. *Science Advances*, *9*(3), eadd8915. https://doi.org/10.1126/sciadv.add8915
1083 Lins, H. F. (2012). *USGS hydro-climatic data network 2009 (HCDN-2009)* (US Geological Survey Fact Sheet 3047
1084 No. 4). Retrieved from https://pubs.usgs.gov/fs/2012/3047/pdf/fs2012-3047.pdf
1085 Malamud, B. D., & Turcotte, D. L. (2006). The applicability of power-law frequency statistics to floods. *Journal of*
1086 *Hydrology*, *322*(1–4), 168–180. https://doi.org/10.1016/j.jhydrol.2005.02.032
1087 Marder, E., & Gallen, S. F. (2023). Climate control on the relationship between erosion rate and fluvial topography.
1088 *Geology*. https://doi.org/10.1130/G50832.1
1089 Molnar, P., Anderson, R. S., Kier, G., & Rose, J. (2006). Relationships among probability distributions of stream
1090 discharges in floods, climate, bed load transport, and river incision. *Journal of Geophysical Research*, *111*,
1091 F02001–F02001. https://doi.org/10.1029/2005JF000310
1092 Nesbitt, S. W., & Anders, A. M. (2009). Very high resolution precipitation climatologies from the Tropical Rainfall
1093 Measuring Mission precipitation radar: TRMM HIGH RESOLUTION PRECIPITATION. *Geophysical*
1094 *Research Letters*, *36*(15), n/a-n/a. https://doi.org/10.1029/2009GL038026
1095 Pitlick, J. (1994). Relation between peak flows, precipitation, and physiography for five mountain regions in the
1096 western USA. *Journal of Hydrology*, *158*, 219–240.
1097 Roe, G. H. (2005). OROGRAPHIC PRECIPITATION. *Annual Review of Earth and Planetary Sciences*, *33*(1), 645–
1098 671. https://doi.org/10.1146/annurev.earth.33.092203.122541
1099 Roe, G. H., Montgomery, D. R., & Hallet, B. (2002). Effects of orographic precipitation variations on the concavity
1100 of steady-state river profiles. *Geology*, *30*(2), 143–146.
1101 Roe, G. H., Montgomery, D. R., & Hallet, B. (2003). Orographic precipitation and the relief of mountain ranges.
1102 *Journal of Geophysical Research*, *108*(B6). https://doi.org/10.1029/2001JB001521

1103 Rossi, M. W., Whipple, K. X., & Vivoni, E. R. (2016). Precipitation and evapotranspiration controls on event-scale
1104 runoff variability in the contiguous United States and Puerto Rico. *Journal of Geophysical Research*, *121*.
1105 https://doi.org/10.1002/2015JF003446
1106 Rossi, M. W., Anderson, R. S., Anderson, S. P., & Tucker, G. E. (2020). Orographic Controls on Subdaily Rainfall
1107 Statistics and Flood Frequency in the Colorado Front Range, USA. *Geophysical Research Letters*, *47*(4).
1108 https://doi.org/10.1029/2019GL085086
1109 Schaefli, B., Rinaldo, A., & Botter, G. (2013). Analytic probability distributions for snow-dominated streamflow:
1110 Snow-Dominated Streamflow Pdfs. *Water Resources Research*, *49*(5), 2701–2713.
1111 https://doi.org/10.1002/wrcr.20234
1112 Schellekens, J., Dutra, E., Weiland, F. S., Minvielle, M., Calvet, J.-C., Decharme, B., et al. (2017). A global water
1113 resources ensemble of hydrological models: the eartH2Observe Tier-1 dataset. *Earth System Data Science*,
1114 *9*(2), 389–413. https://doi.org/10.5194/essd-9-389-2017
1115 Scherler, D., DiBiase, R. A., Fisher, G. B., & Avouac, J.-P. (2017). Testing monsoonal controls on bedrock river
1116 incision in the Himalaya and Eastern Tibet with a stochastic-threshold stream power model. *Journal of*
1117 *Geophysical Research: Earth Surface*, *122*, 1389–1429. https://doi.org/10.1002/2016JF004011
1118 Schmied, H., Eisner, S., Franz, D., Wattenbach, M., Portmann, F. T., Flörke, M., & Döll, P. (2014). Sensitivity of
1119 simulated global-scale freshwater fluxes and storages to input data, hydrological model structure, human
1120 water use and calibration. *Hydrology and Earth System Sciences*, *18*(9), 3511–3538.
1121 https://doi.org/10.5194/hess-18-3511-2014
1122 Schmied, H., Cáceres, D., Eisner, S., Flörke, M., Herbert, C., Niemann, C., et al. (2020). The global water resources
1123 and use model WaterGAP v2.2d: Model description and evaluation. *Geoscientific Model Development*, *14*,
1124 1037–1079. https://doi.org/10.5194/gmd-2020-225
1125 Schwanghart, W., & Scherler, D. (2014). Short Communication: TopoToolbox 2 - MATLAB based software for
1126 topographic analysis and modeling in Earth surface sciences. *Earth Surface Dynamics*, *2*, 1–7.
1127 https://doi.org/10.5194/esurf-2-1-2014
1128 Shen, H., Lynch, B., Poulsen, C. J., & Yanites, B. J. (2021). A modeling framework (WRF-Landlab) for simulating
1129 orogen-scale climate-erosion coupling. *Computers & Geosciences*, *146*, 104625.
1130 https://doi.org/10.1016/j.cageo.2020.104625

1131 Shobe, C. M., Tucker, G. E., & Anderson, R. S. (2016). Hillslope-derived blocks retard river incision. *Geophysical*
1132 *Research Letters*, *43*(10), 5070–5078. https://doi.org/10.1002/2016GL069262
1133 Sivapalan, M., Jothityangkoon, C., & Menabde, M. (2002). Linearity and nonlinearity of basin response as a
1134 function of scale: Discussion of alternative definitions: TECHNICAL NOTE. *Water Resources Research*,
1135 *38*(2), 4-1-4–5. https://doi.org/10.1029/2001WR000482
1136 Smith, R. B. (1979). The Influence of Mountains on the Atmosphere. In B. Saltzman (Ed.), *Advances in Geophysics*
1137 (Vol. 21, pp. 87–230). Elsevier. https://doi.org/10.1016/S0065-2687(08)60262-9
1138 Smith, R. B., & Barstad, I. (2004). A Linear Theory of Orographic Precipitation. *Journal of the Atmospheric*
1139 *Sciences*, *61*(12), 1377–1391. https://doi.org/10.1175/1520-0469(2004)061<1377:ALTOOP>2.0.CO;2
1140 Snyder, N. P., Whipple, K. X., Tucker, G. E., & Merrits, D. J. (2003). Importance of a stochastic distribution of
1141 floods and erosion thresholds in the bedrock river incision problem. *Journal of Geophysical Research*,
1142 *108*(B2). https://doi.org/10.1029/2001JB001655
1143 Stolar, D. B., Willett, S. D., & Roe, G. H. (2006). Climatic and tectonic forcing of a critical orogen. In S. D. Willett,
1144 N. Hovius, M. T. Brandon, & D. Fisher (Eds.), *Tectonics, climate, and landscape evolution* (Vol. 398, pp.
1145 241–250). Geological Society of America.
1146 Trenberth, K. E., Dai, A., Rasmussen, R. M., & Parsons, D. B. (2003). The Changing Character of Precipitation.
1147 *Bulletin of the American Meteorological Society*, *84*(9), 1205–1218. https://doi.org/10.1175/BAMS-84-9-
1148 1205
1149 Tucker, G. E. (2004). Drainage basin sensitivity to tectonic and climatic forcing: Implications of a stochastic model
1150 for the role of entrainment and erosion thresholds. *Earth Surface Processes and Landforms*, *29*, 185–204.
1151 https://doi.org/10.1002/esp.1020
1152 Tucker, G. E., & Bras, R. L. (2000). A stochastic approach to modeling the role of rainfall variability in drainage
1153 basin evolution. *Water Resources Research*, *36*(7), 1953–1964.
1154 Walter, M. T., Brooks, E. S., McCool, D. K., King, L. G., Molnau, M., & Boll, J. (2005). Process-based snowmelt
1155 modeling: does it require more input data than temperature-index modeling? *Journal of Hydrology*, *300*(1–
1156 4), 65–75. https://doi.org/10.1016/j.jhydrol.2004.05.002
1157 Whipple, K. X. (2009). Landscape texture set to scale. *Nature*, *460*, 468–469.

1158 Whipple, K. X., & Meade, B. (2004). Controls on the strength of coupling among climate, erosion, and deformation
1159 in two-sided, frictional orogenic wedges at steady state. *Journal of Geophysical Research*, *109*, F01011–
1160 F01011. https://doi.org/10.1029/2003JF000019
1161 Whipple, K. X., & Tucker, G. E. (1999). Dynamics of the stream-power river incision model: Implications for
1162 height limits of mountain ranges, landscape response timescales, and research needs. *Journal of*
1163 *Geophysical Research*, *104*(B8), 17661–17674.
1164 Whipple, K. X., Kirby, E., & Brocklehurst, S. H. (1999). Geomorphic limits to climate-induced increases in
1165 topographic relief. *Nature*, *401*, 39–43.
1166 Whipple, K. X., Hancock, G. S., & Anderson, R. S. (2000). River incision into bedrock: Mechanics and relative
1167 efficacy of plucking, abrasion, and cavitation. *Geology*, *112*(3), 490–503.
1168 Whipple, K. X., DiBiase, R. A., Crosby, B., & Johnson, J. P. L. (2022). Bedrock Rivers. In J. (Jack) F. Shroder
1169 (Ed.), *Treatise on Geomorphology (Second Edition)* (pp. 865–903). Oxford: Academic Press.
1170 https://doi.org/10.1016/B978-0-12-818234-5.00101-2
1171 Whittaker, A. C. (2012). How do landscapes record tectonics and climate. *Lithosphere*, *4*, 160–164.
1172 Willett, S. D. (1999). Orogeny and orography: The effects of erosion on the structure of mountain belts. *Journal of*
1173 *Geophysical Research*, *104*(B12), 28,957-28,981.
1174 Wilson, P. S., & Toumi, R. (2005). A fundamental probability distribution for heavy rainfall. *Geophysical Research*
1175 *Letters*, *32*(14). https://doi.org/10.1029/2005GL022465
1176 Wobus, C. W., Whipple, K. X., Kirby, E., Snyder, N. P., Johnson, J., Spyropolou, K., et al. (2006). Tectonics from
1177 topography: Procedures, promise, and pitfalls. In S. D. Willett, N. Hovius, M. T. Brandon, & D. Fisher
1178 (Eds.), *Tectonics, climate, and landscape evolution* (Vols. 1–398, pp. 55–74). Boulder, CO: The Geological
1179 Society of America.

1180

Figure 1.

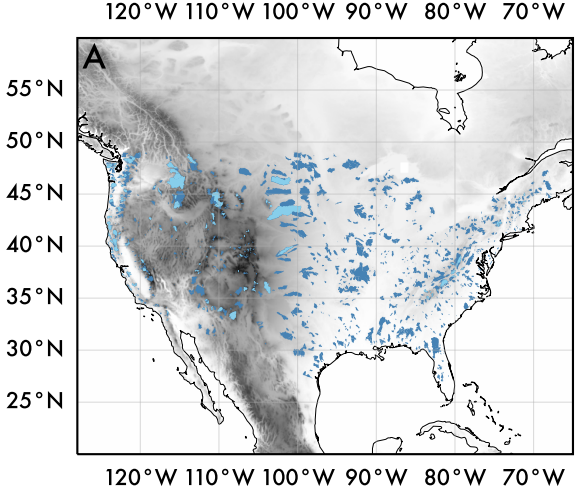
A
120°W 110°W 100°W 90°W 80°W 70°W
55°N
50°N
45°N
40°N
35°N
30°N
25°N
Gages-II Reference
Filtered HCDN-2009

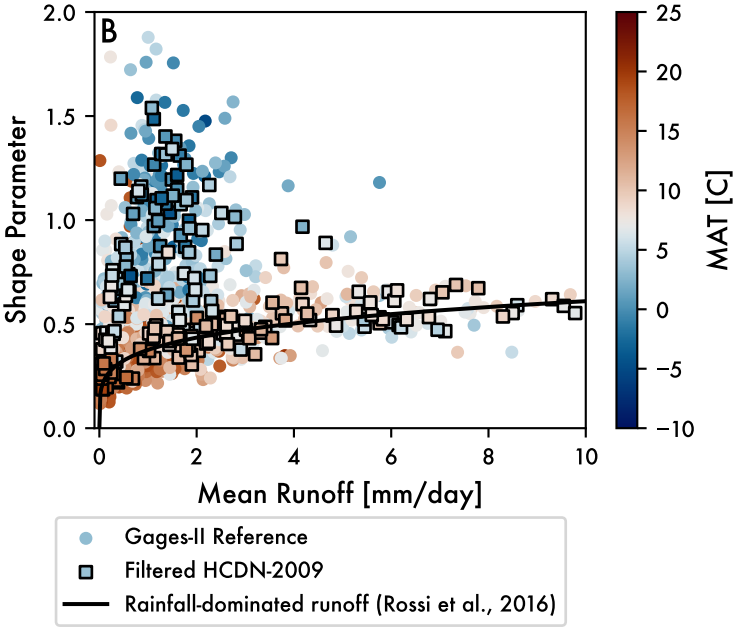
B
Shape Parameter
2.0
1.5
1.0
0.5
0.0
0
2
4
6
8
10
Mean Runoff [mm/day]
MAT [C]
25
20
15
10
5
0
−5
−10
Gages-II Reference
Filtered HCDN-2009
Rainfall-dominated runoff (Rossi et al., 2016)

Figure 2.

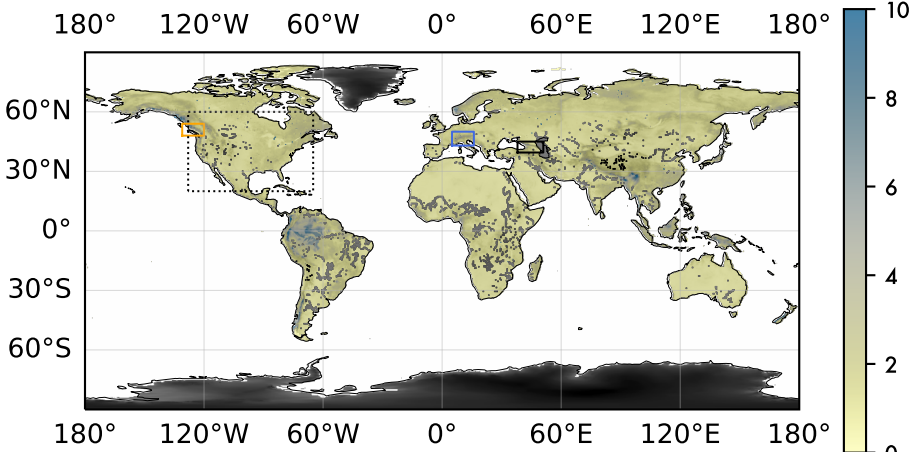
180°
120°W
60°W
0°
60°E
120°E
180°
60°N
30°N
0°
30°S
60°S
Mean Runoff [mm/day]
0
2
4
6
8
10

Figure 3.

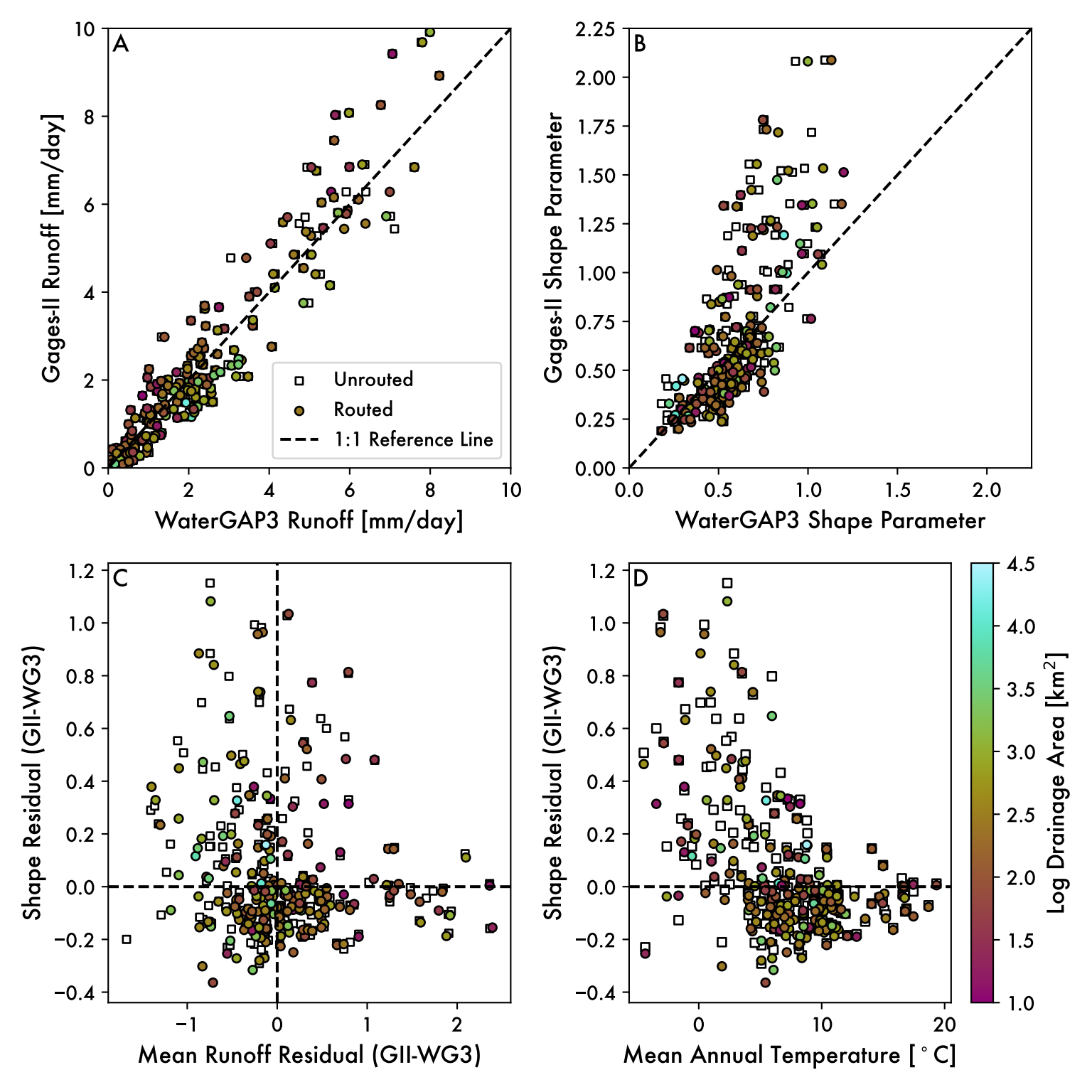
A
Gages-II Runoff [mm/day]
WaterGAP3 Runoff [mm/day]
Unrouted
Routed
1:1 Reference Line
B
Gages-II Shape Parameter
WaterGAP3 Shape Parameter
C
Shape Residual (GII-WG3)
Mean Runoff Residual (GII-WG3)
D
Shape Residual (GII-WG3)
Mean Annual Temperature [°C]
Log Drainage Area [km²]

Figure 4.

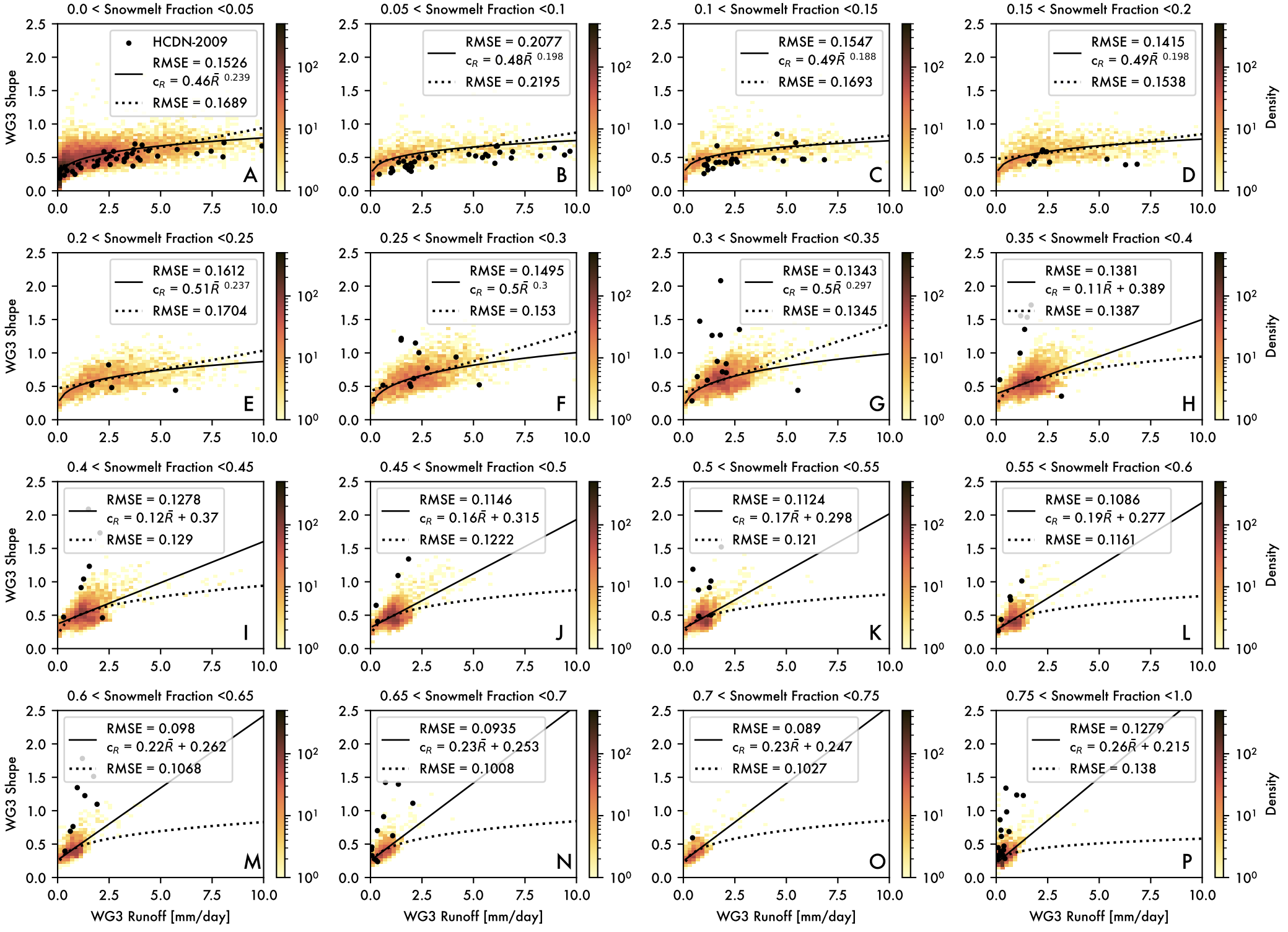
0.0 < Snowmelt Fraction <0.05
HCDN-2009
RMSE = 0.1526
$c_R = 0.46\bar{R}^{0.239}$
RMSE = 0.1689
A
0.05 < Snowmelt Fraction <0.1
RMSE = 0.2077
$c_R = 0.48\bar{R}^{0.198}$
RMSE = 0.2195
B
0.1 < Snowmelt Fraction <0.15
RMSE = 0.1547
$c_R = 0.49\bar{R}^{0.188}$
RMSE = 0.1693
C
0.15 < Snowmelt Fraction <0.2
RMSE = 0.1415
$c_R = 0.49\bar{R}^{0.198}$
RMSE = 0.1538
D
0.2 < Snowmelt Fraction <0.25
RMSE = 0.1612
$c_R = 0.51\bar{R}^{0.237}$
RMSE = 0.1704
E
0.25 < Snowmelt Fraction <0.3
RMSE = 0.1495
$c_R = 0.5\bar{R}^{0.3}$
RMSE = 0.153
F
0.3 < Snowmelt Fraction <0.35
RMSE = 0.1343
$c_R = 0.5\bar{R}^{0.297}$
RMSE = 0.1345
G
0.35 < Snowmelt Fraction <0.4
RMSE = 0.1381
$c_R = 0.11\bar{R} + 0.389$
RMSE = 0.1387
H
0.4 < Snowmelt Fraction <0.45
RMSE = 0.1278
$c_R = 0.12\bar{R} + 0.37$
RMSE = 0.129
I
0.45 < Snowmelt Fraction <0.5
RMSE = 0.1146
$c_R = 0.16\bar{R} + 0.315$
RMSE = 0.1222
J
0.5 < Snowmelt Fraction <0.55
RMSE = 0.1124
$c_R = 0.17\bar{R} + 0.298$
RMSE = 0.121
K
0.55 < Snowmelt Fraction <0.6
RMSE = 0.1086
$c_R = 0.19\bar{R} + 0.277$
RMSE = 0.1161
L
0.6 < Snowmelt Fraction <0.65
RMSE = 0.098
$c_R = 0.22\bar{R} + 0.262$
RMSE = 0.1068
M
0.65 < Snowmelt Fraction <0.7
RMSE = 0.0935
$c_R = 0.23\bar{R} + 0.253$
RMSE = 0.1008
N
0.7 < Snowmelt Fraction <0.75
RMSE = 0.089
$c_R = 0.23\bar{R} + 0.247$
RMSE = 0.1027
O
0.75 < Snowmelt Fraction <1.0
RMSE = 0.1279
$c_R = 0.26\bar{R} + 0.215$
RMSE = 0.138
P
WG3 Shape
WG3 Runoff [mm/day]
Density

Figure 5.

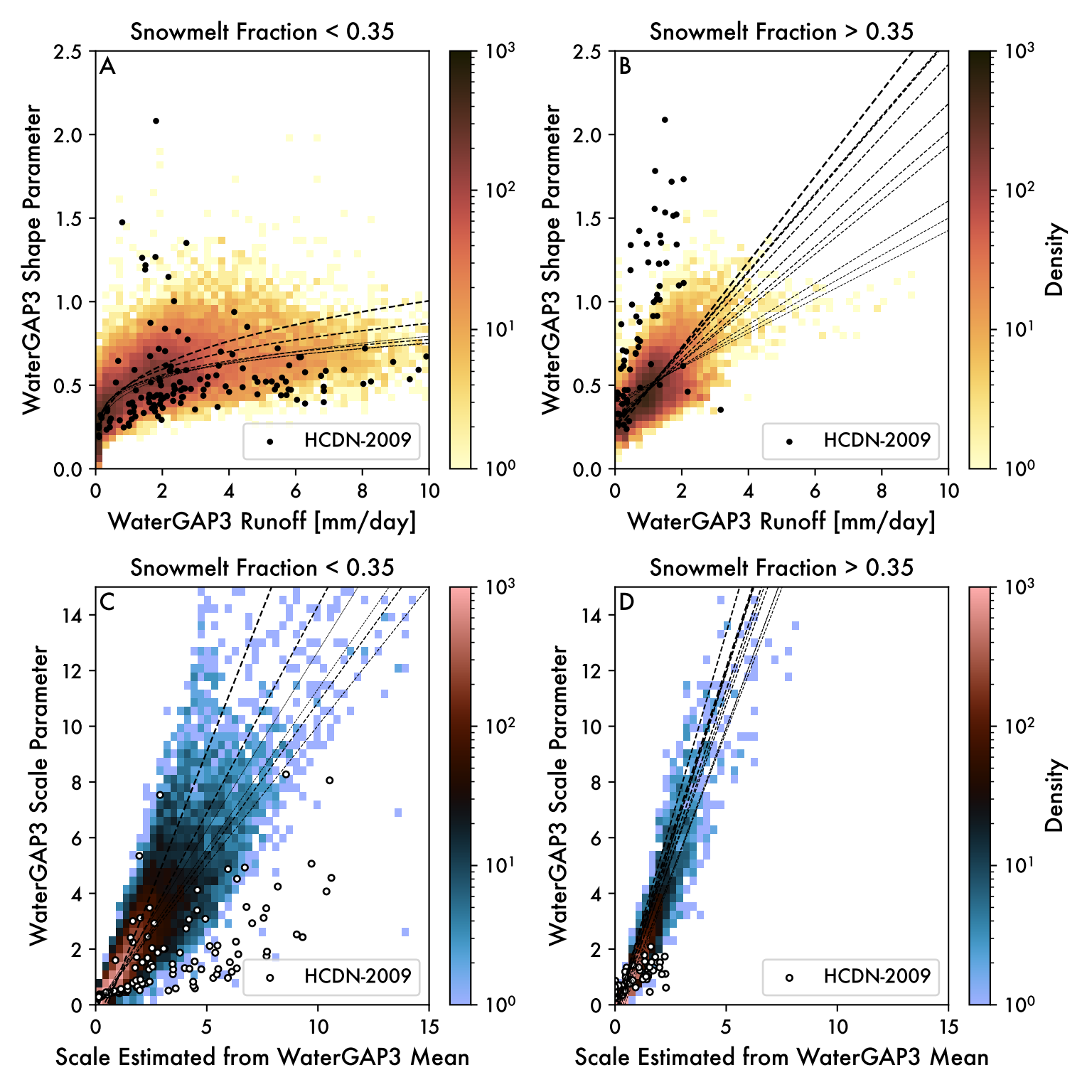
Snowmelt Fraction < 0.35
Snowmelt Fraction > 0.35
A
B
C
D
WaterGAP3 Shape Parameter
WaterGAP3 Scale Parameter
WaterGAP3 Runoff [mm/day]
Scale Estimated from WaterGAP3 Mean
HCDN-2009
Density

Figure 6.

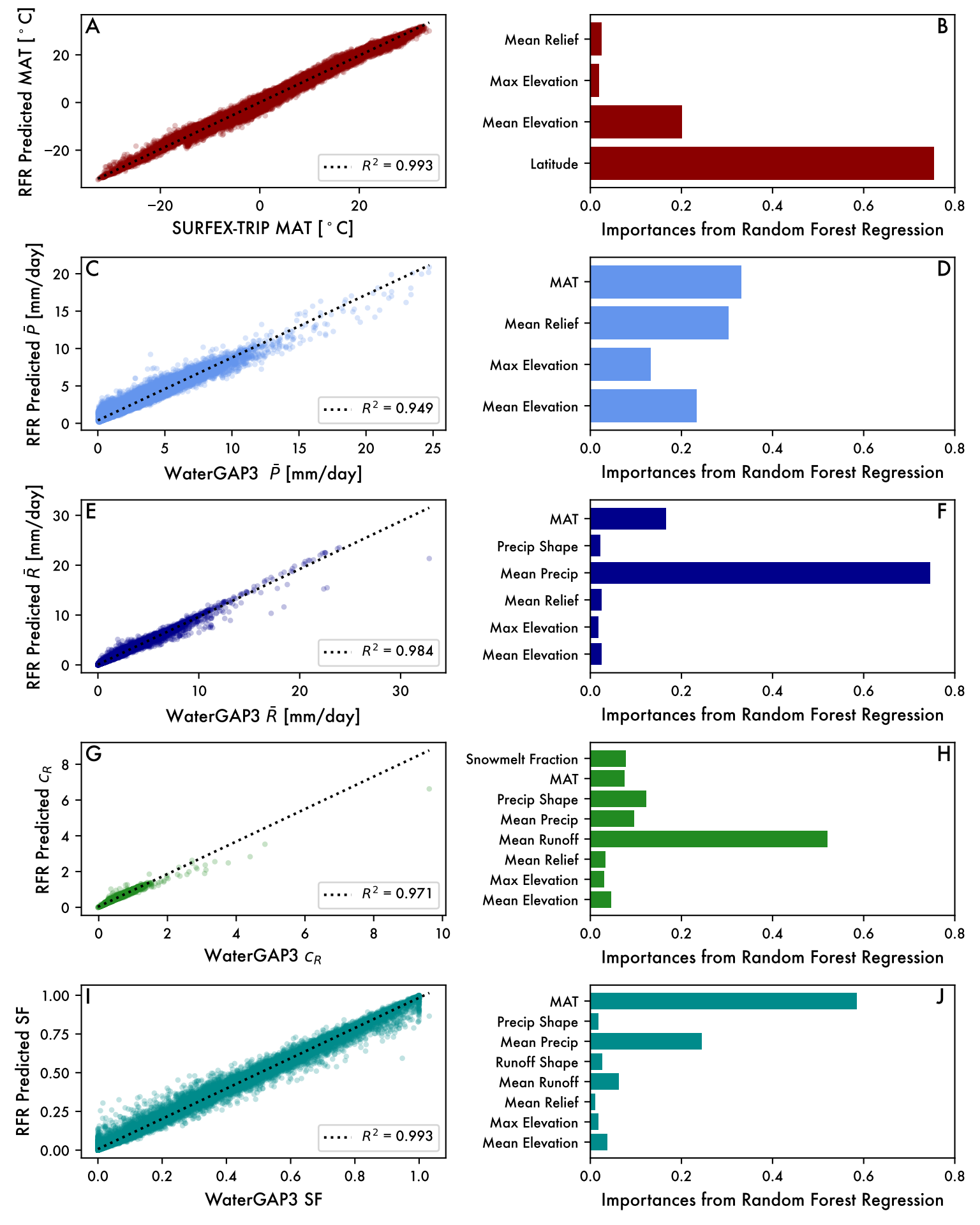
A
RFR Predicted MAT [° C]
SURFEX-TRIP MAT [° C]
R^2 = 0.993
B
Mean Relief
Max Elevation
Mean Elevation
Latitude
Importances from Random Forest Regression
C
RFR Predicted $\bar{P}$ [mm/day]
WaterGAP3 $\bar{P}$ [mm/day]
R^2 = 0.949
D
MAT
Mean Relief
Max Elevation
Mean Elevation
Importances from Random Forest Regression
E
RFR Predicted $\bar{R}$ [mm/day]
WaterGAP3 $\bar{R}$ [mm/day]
R^2 = 0.984
F
MAT
Precip Shape
Mean Precip
Mean Relief
Max Elevation
Mean Elevation
Importances from Random Forest Regression
G
RFR Predicted c_R
WaterGAP3 c_R
R^2 = 0.971
H
Snowmelt Fraction
MAT
Precip Shape
Mean Precip
Mean Runoff
Mean Relief
Max Elevation
Mean Elevation
Importances from Random Forest Regression
I
RFR Predicted SF
WaterGAP3 SF
R^2 = 0.993
J
MAT
Precip Shape
Mean Precip
Runoff Shape
Mean Runoff
Mean Relief
Max Elevation
Mean Elevation
Importances from Random Forest Regression

Figure 7.

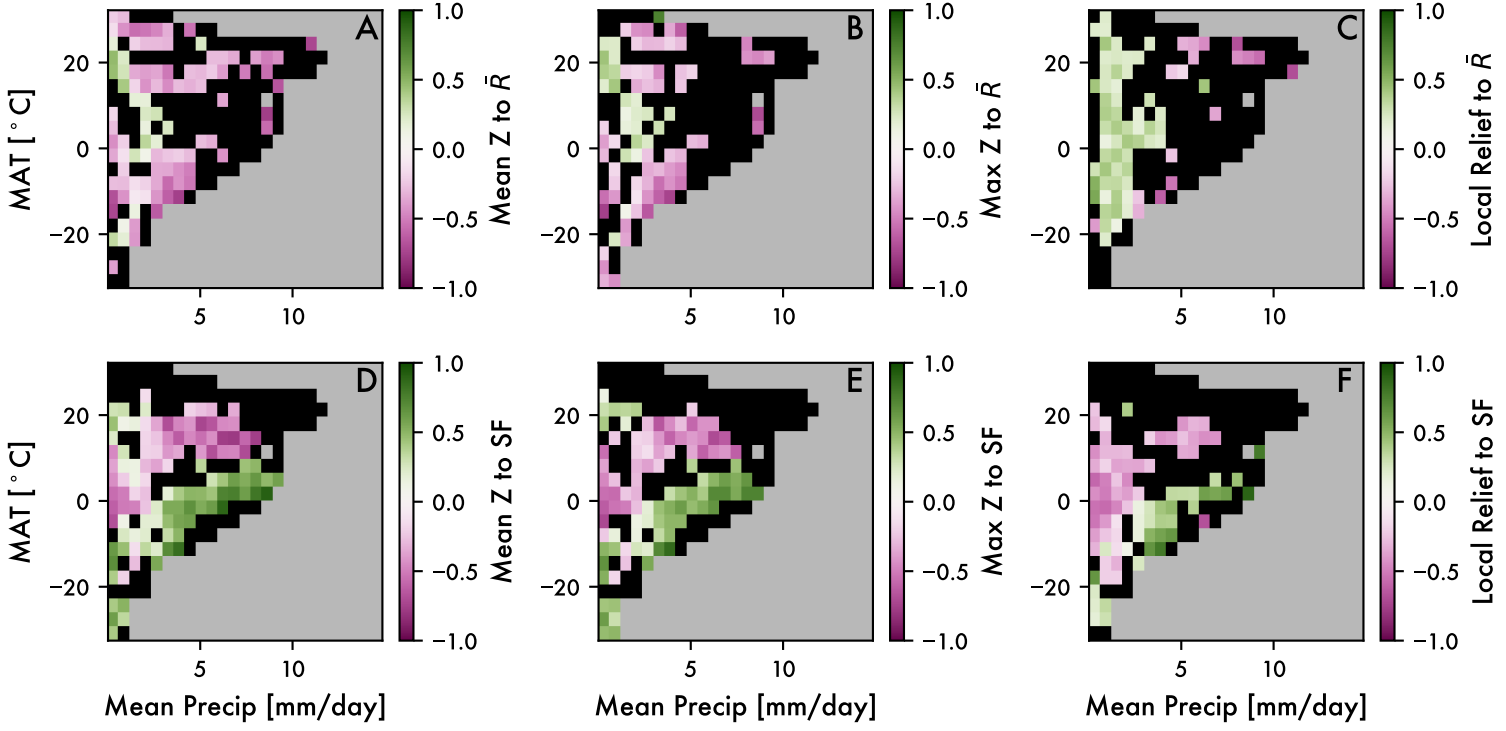
A
B
C
D
E
F
MAT [° C]
Mean Precip [mm/day]
Mean Z to $\bar{R}$
Max Z to $\bar{R}$
Local Relief to $\bar{R}$
Mean Z to SF
Max Z to SF
Local Relief to SF
20
0
−20
5
10
1.0
0.5
0.0
−0.5
−1.0

Figure 8.

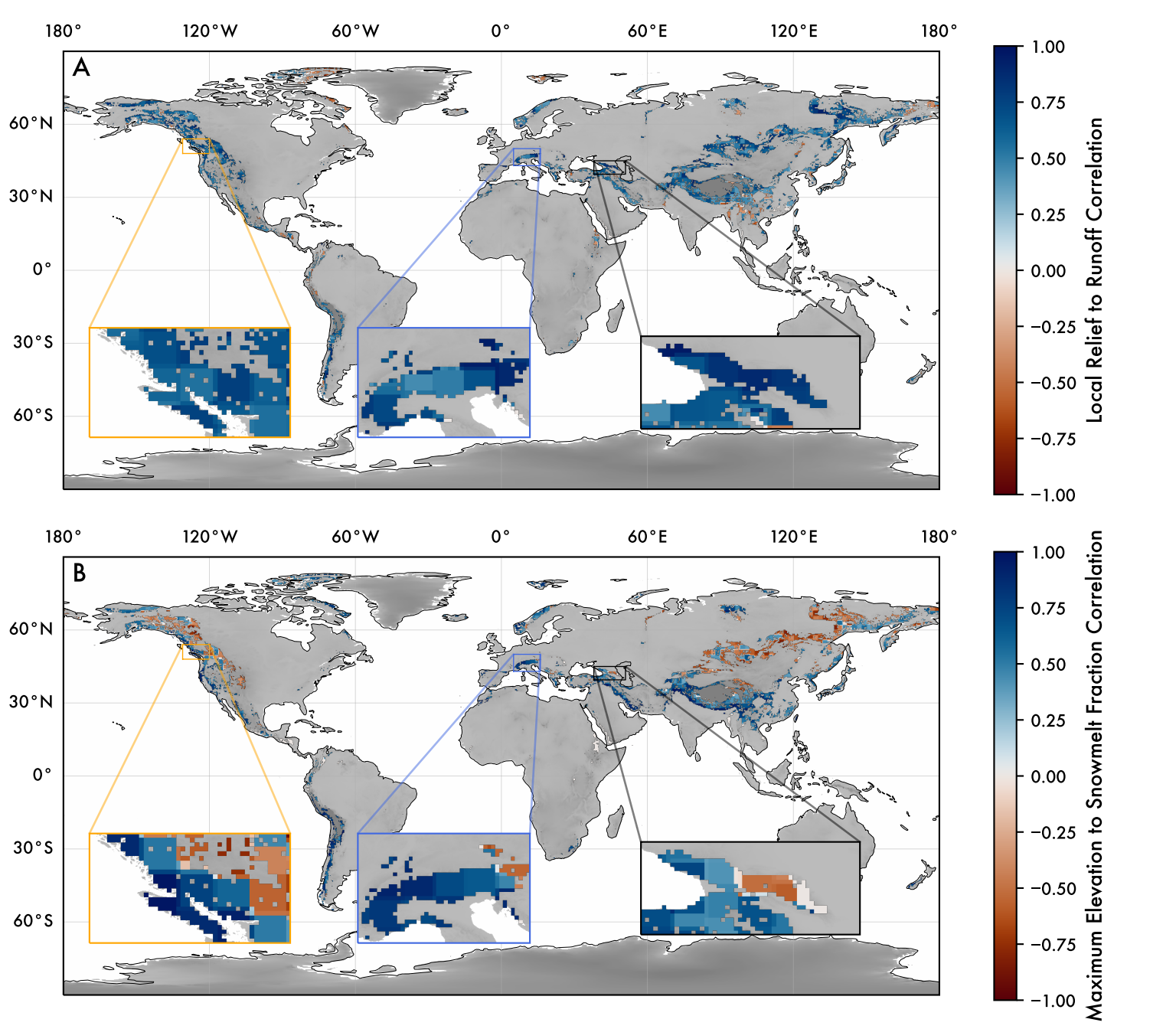
A
B
180°
120°W
60°W
0°
60°E
120°E
180°
60°N
30°N
0°
30°S
60°S
1.00
0.75
0.50
0.25
0.00
−0.25
−0.50
−0.75
−1.00
Local Relief to Runoff Correlation
Maximum Elevation to Snowmelt Fraction Correlation

Figure 9.

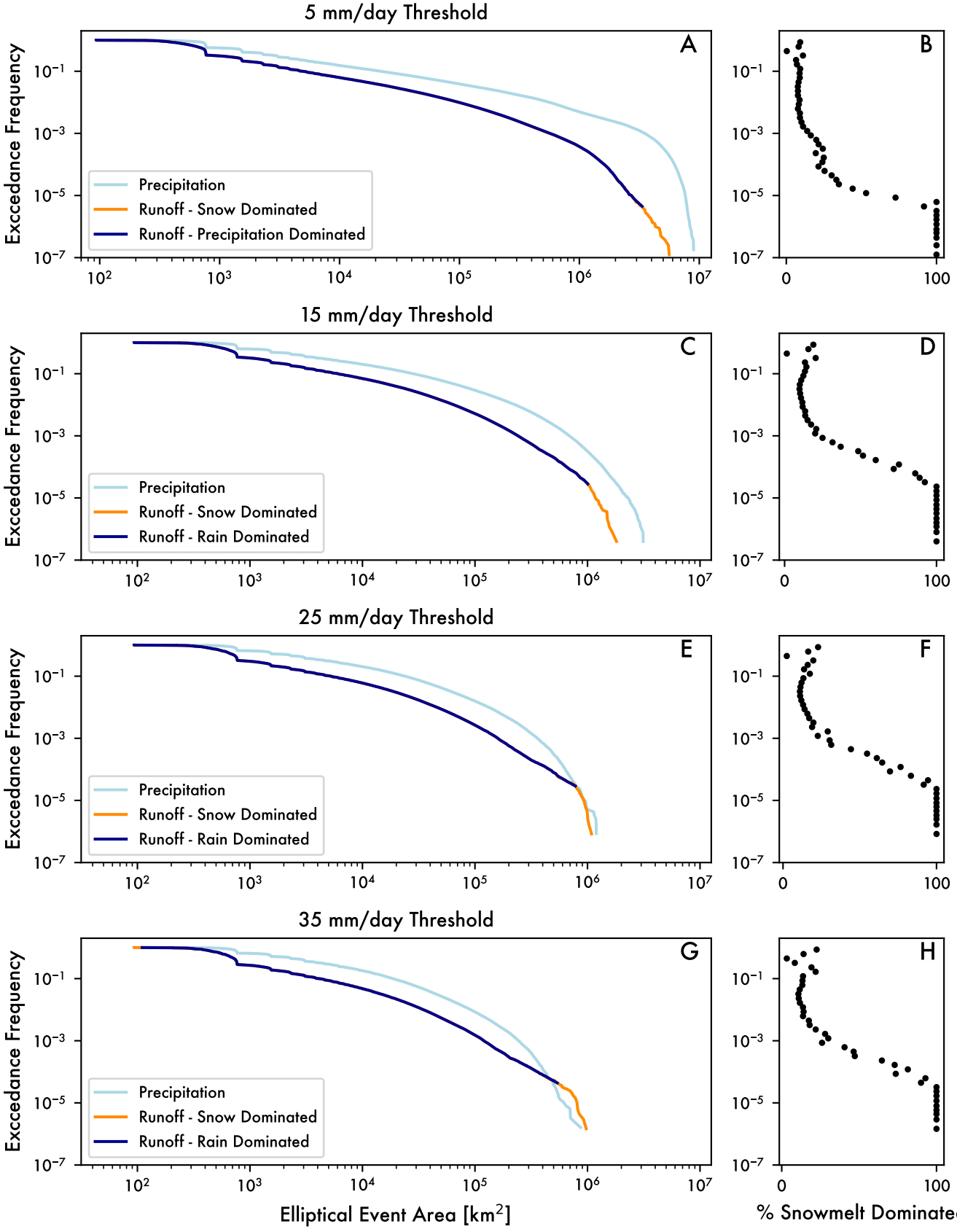
5 mm/day Threshold
A
B
Exccedance Frequency
Precipitation
Runoff - Snow Dominated
Runoff - Precipitation Dominated
15 mm/day Threshold
C
D
Runoff - Rain Dominated
25 mm/day Threshold
E
F
35 mm/day Threshold
G
H
Elliptical Event Area [km^2]
% Snowmelt Dominated

Figure 10.

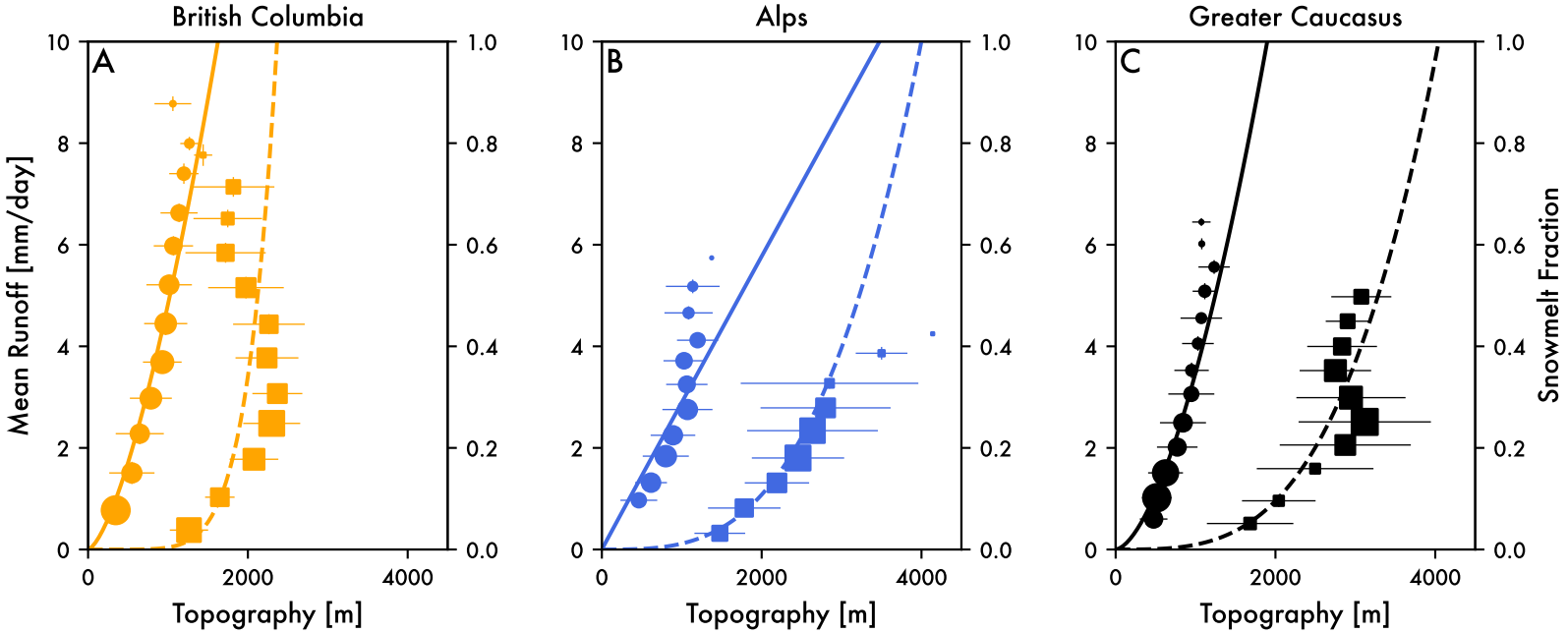

Local Relief to Mean Runoff
$\bar{R}$ = 1.54e-04 * Rlf $^{1.499}$; RMSE = 1.74
Max. Elev. to Snowmelt Fraction
SF = 2.28e-22 * Max Z $^{6.415}$; RMSE = 1.18

Local Relief to Mean Runoff
$\bar{R}$ = 2.99e-03 * Rlf $^{0.995}$; RMSE = 1.04
Max. Elev. to Snowmelt Fraction
SF = 2.64e-12 * Max Z $^{3.214}$; RMSE = 0.22

Local Relief to Mean Runoff
$\bar{R}$ = 3.91e-05 * Rlf $^{1.65}$; RMSE = 1.15
Max. Elev. to Snowmelt Fraction
SF = 9.33e-13 * Max Z $^{3.335}$; RMSE = 0.35

Figure 11.

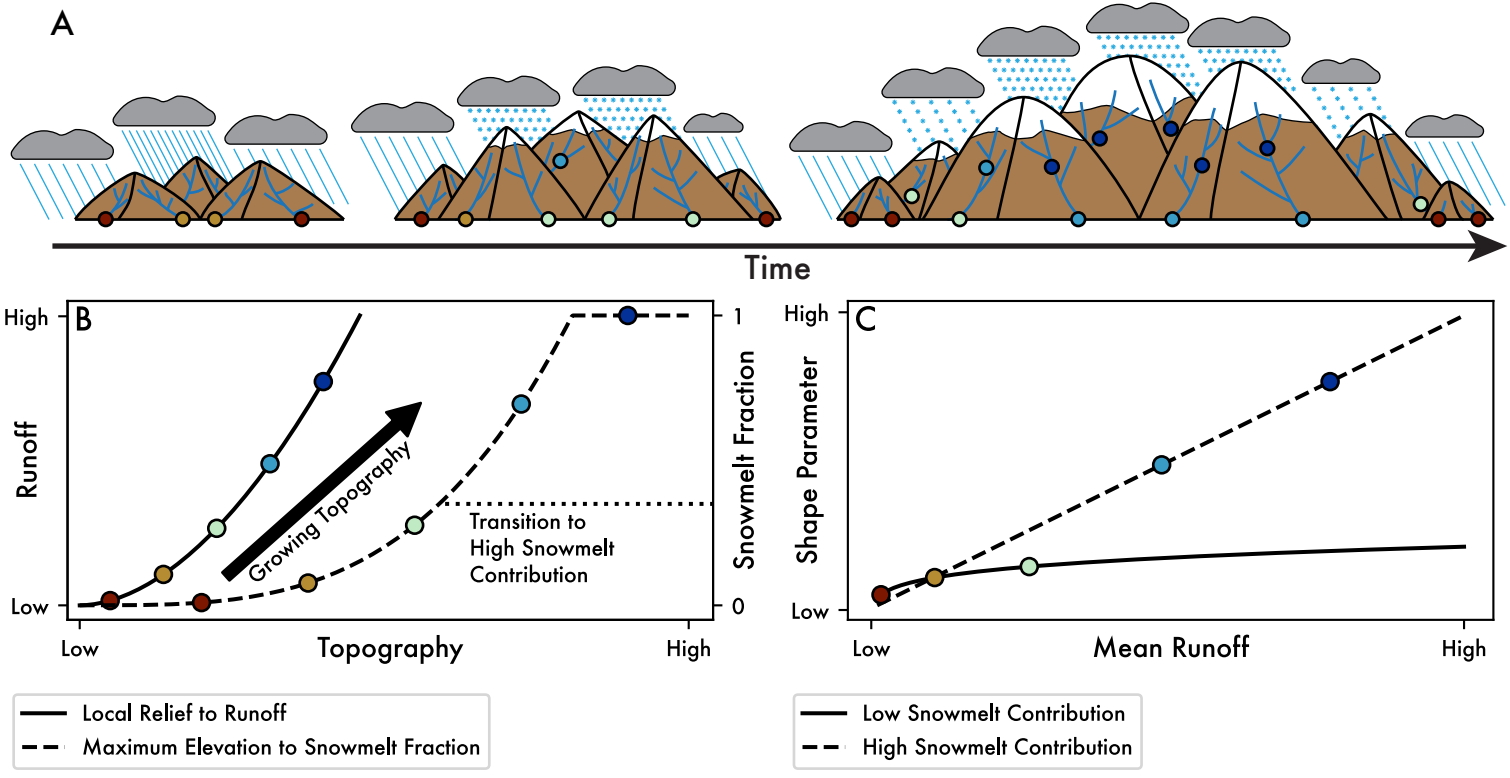
A
Time
B
High
Low
Runoff
Growing Topography
Transition to
High Snowmelt
Contribution
1
0
Snowmelt Fraction
Low
Topography
High
C
High
Low
Shape Parameter
Low
Mean Runoff
High
Local Relief to Runoff
Maximum Elevation to Snowmelt Fraction
Low Snowmelt Contribution
High Snowmelt Contribution